Memristor for Radiation sensing

Muna M. Darweesh

MSc. Thesis

April 2017

جامعة خليفة
KHALIFA UNIVERSITY

A thesis submitted to Khalifa University of Science, Technology and Research in accordance with the requirements of the degree of Master of Science in Electrical and Computer Engineering in the Department of Electrical and Computer Engineering.

Memristor for Radiation sensing

by

Muna M. Darweesh

A thesis submitted in partial fulfillment of the
requirements for the degree of

Master of Science in Electrical and Computer Engineering

at

Khalifa University

Thesis Committee

Dr. Baker Mohammad
(Supervisor & Examiner),
Khalifa University

Dr.Maguy Abi Jaoude
(Co-Supervisor),
Khalifa University

Dr. George Wesley Hitt
(Co-Supervisor),
Khalifa University

Dr. Yousof Al-Hammadi
(Committee Chair),
Khalifa University

Dr. Dirar Mohammad Al Homouz
(Examiner),
Khalifa University

April 2017

جامعة خليفة
KHALIFA UNIVERSITY

Abstract

Muna Darweesh, "**Memristor for radiation sensing**", M.Sc. Thesis, M. Sc. in Electrical and Computer Engineering, Department of Electrical and Computer Engineering, Khalifa University of Science, Technology and Research, United Arab Emirates, April 2017.

The development of environmental radiation monitoring and therapy have been influenced by the advancements of the semiconductor industry. Semiconductor based detectors such as Silicon and Metal Oxide (MOS) are known for both their low cost as well as miniature sizes. Nevertheless, the problem with MOS transistor is that the radiation induces charges which get trapped in the gate oxide. In specific, due to irradiation, the turned-on transistor reduces the threshold voltage which prevents the transistor from switching off back again, hence greatly damaging the circuitry. However, low cost, scalable, and repeatable detectors which can both operate at low voltage as well as possess natural behavior in the presence of radiation are a necessity. In this case, Memristor is considered an option due to the wide array of favorable characteristics it retains. Its metal-insulator-metal structure which is similar to the MOS detector promotes the memristor to be investigated as a radiation sensor. Furthermore, the scalability, thickness scaling, behavior repeatability and low operating power of the memristor results in emphasizing the necessity of investigating it as an option to detect the ionizing radiation.

Therefore, a genuine classification for the existing radiation detectors have been achieved as a result of a comprehensively conducted review. This new classification is based on the collecting mechanisms, in specific the output of the detector indicates the effect of irradiation. Furthermore, in this research, a solution for the MOS transistor issue is proposed by investigating the electrical characteristics of a micro-thick memristor as a possible radiation sensor. Novel protocols for electrical testing have been conducted in order to study the memristor key features, such as the switching mechanisms. In addition, the set process along with its time dependency model as well as the reset process, retention and endurance are investigated for the first time in the literature for a micro-thick memristor. Experimental results proved that the R_{OFF}/R_{ON} is 10^7 which indicates a good noise margin. It also demonstrated that a high endurance of more than 50 cycles has been detected. Further, it is the first micro-thick memristor to have repeatable switching mechanism indicated by its capability to be set at 0.6V and reset at -0.2V. Finally, statistical analysis for the electrical behavior prior, during and after ionizing irradiation is executed.

Indexing Terms: Electrochemical metallization, Sol-gel, Thin film, sensing, micro-thick memristor, Titanium dioxide, ionizing electromagnetic radiation, gamma rays

Acknowledgement

First of all, I would like to thank my supervisors, Dr. Baker Mohammad, Dr. Maguy Abi Jaoude and Dr. George Wesley Hitt for their attentive support and dedicated guidance. Also, special thanks to the amazing research associate “Lama” for her incredible support and help.

I would like to express my sincere gratitude to Dr. Hasna for her help during this project. A special thanks, for the astonishing research associate “Zainab Al Noamani” for her help and her assistant in conducting the nuclear experiments.

Also, I would express my deep gratitude for my parents, and my sister and my brothers for their greet supports

For all my friends, and my colleagues, many thanks for your endless encouragements and support.

Declaration and Copyright

Declaration

I declare that the work in this thesis was carried out in accordance with the regulations of Khalifa University of Science, Technology and Research. The work is entirely my own except where indicated by special reference in the text. Any views expressed in the thesis are those of the author and in no way represent those of Khalifa University of Science, Technology and Research. No part of the thesis has been presented to any other university
for any degree.

Author Name: _____Muna Darweesh_____

Author Signature: _____Muna_____

Date: _____30/4/2017_____

Copyright ©

Table of Contents

List of Figures

List of Tables

List of symbols

γ	Gamma
Gy	Gray
I_0	Gamma ray intensity
μ_L	Mass attenuation constant
L	Absorber thickness
R	Roentgen
Li	Lithium
Silicon (Lithium)	Si (Li)
K	Kelvin
R_{off}	Off state resistance
R_{on}	On state resistance
V_{set}	Set voltage
I_{reset}	Reset current
V_{reset}	Reset voltage
L	Mean free path

List of Abbreviations

SNR	Signal to noise ratio
MOSFET	Metal oxide semiconductor field-effect transistor
IC	Ionization channel
PC	Proportional counter
GM	Geiger Miller
HRS	High resistance state
LRS	Low resistance state
CC	Compliance current

Introduction

1.1 Research Motivations

Gamma ionizing radiation is extensively used in numerous fields such as environmental monitoring, medical imaging, waste treatment, military, and consumer products. Further benefits involve the food sterilization in which exposing the food to the radiation eradicates the harmful organisms. However, radiation exposure to the human body may cause serious consequences, which can cause cell mutation and malfunction due to the extensive ionization to the human cells.

Consequently, radiation dosimetry and protection fields flourish and can be classified based on their detecting mechanisms namely: the current collecting detector (i.e. Geiger miller), the heat collecting (i.e calorimeter) detector, the light collecting (scintillator), the defect collecting (photographic film) and the charge collecting detector (i.e. semiconductor), which are all utilized in radiation detection. One of these detectors is the semiconductor-based which attracts researchers' interest specifically when talking about the metal oxide semiconductor (MOS). MOS dosimeters are known for their high accuracy, small size and simple structure. Typically, these dosimeter can be active or passive radiation detectors. Despite the advantages, some detectors require the high operating voltage, time consuming and expensive read-out system, low resolution as well as high dependency on the surrounding environment. One example is that when the ionizing radiation passes through the nMOSFET, the threshold voltage is shifted to lower levels since the trapped charges that are induced by the radiation get accumulated in the gate oxide. Consequently, the nMOS transistor cannot be turned off even if the supply voltage is removed.

Extensive development and advancement in the radiation dosimetry is highly needed to address the aforementioned issues. The need for a repeatable, low power, as well as a scalable dosimeter that comprises a reliable functionality is critical. The Memristor device characterized by its metal-insulator-metal structure is quite similar to the MOS detector. The memristor's unique resistive switching, working mechanisms and high endurance, all these electrical characteristics, promote such device to be studied for its sensing capability.

The potential of having the memristor fabricated at higher thicknesses, from the nano-scale to micro-scale, of what have been reported in the literature provides sufficient room for the radiation to interact with the materials and opens new direction for memristor applications.

Around 30 studies in the literature presented that nanoscale memristors have been studied for radiation hardness. Nonetheless, only one article studies the memristor for its sensing applications at the micro-scale. Such research gap for this type of study is another major motivation for conducting this innovative research.

Thus, in this research the electrical characteristics of the micro-thick memristor are studied to investigate this device as ionizing radiation sensor.

1.2 Thesis contributions

- Develop a testing protocol for microscale memristor.
- Define Retention test and endurance protocols.
- Repeatable switching behavior micro-thick memristor with low operating voltage range.
- Study the time response for set and reset process and the set modeling.
- The highest R_{OFF}/ R_{ON} reported in micro-thick memristor which is $10^{7.}$
- Initial insights to the low resistance state modeling for the retention test.
- Literature review on existing technologies for gamma-ray sensing.

1.3 Thesis publications

Under review

M. Darweesh member, G. Wesly Hitt, M. Abi Jaoude, L. Mahmoud, B. Mohammad, "Ionizing Radiation detectors: different approaches and a new emerging detector" in *IEEE transaction on Nuclear science*

Accepted

L. Mahmoud, M. Abi Jaoude, M. Darweesh, H. Abunahla, G.Wesly Hitt and B. Mohammad, "Low-Power and Highly Stable Microscale TiO2 Memristors for Gamma-Ray Sensing", The International Conference on Memristive Materials, Devices & Systems (MEMRISYS), 2017.

1.4 Thesis outline

Chapter 2 provides an introductory about the electromagnetic ionizing radiation, their applications, their advantages and disadvantages. Moreover, it gives novel classification for the existing radiation detector. Finally, an emerging radiation detector "Memristor" is discussed.

Chapter 3 gives a short description for the fabrication process of the proposed memristor. Furthermore, the chapter presents the electrical experimental results without, during and after exposure to gamma radiation, and discusses the observations and findings. Moreover, the sensing capability of the memristor is studied through the electrical characterization of the memristor before, during and after gamma irradiation.

The last chapter, chapter 4, gives concluding remarks based on the experimental results and suggests possible future works.

Chapter2
A Survey on Electromagnetic Ionizing Radiation, Radiation Interactions and Dosimetry

In this chapter, a background on radiation, radiation interactions and radiation dosimetry are illustrated.

2.1 Electromagnetic Radiation

Radiation is a term that combines electrons, particles, electromagnetic waves, neutrons and protons. Radiation can be divided into types which are nonionizing and ionizing radiation, as shown in Figure 2.1. The non-ionizing radiation cannot ionize the matter [1], whereas the ionizing energy it can ionize or remove electron from the atom [1, 2]. The ionizing incident energy interact with the matter in two distinct ways, i.e direct and indirect types, depending on whether the radiation is charged particles or not [2]. For the direct one, the charged particles, such as electrons, interact directly through the coulomb interactions with the orbital electrons of the target atoms. For the indirect one, the charged particle is released in the medium first. Then because of the deposited energy, the coulomb interactions occur with orbital electrons of the targeted atoms [1]. One type of ionizing electromagnetic radiation is the photon. Gamma (γ)-ray is a well-known ionizing radiation. It is generated from nuclear transitions. They act as massless and uncharged particles. It has high energy between 10keV to 3 MeV [3], and it travels at the speed of the light in the vacuum [4]. It is located at the end of the electromagnetic spectrum and its frequency range is more than 10^{20} Hz [1], as shown in Figure 2.2. Thus, with these various characteristics, $\gamma -$ ray is employed in different applications.

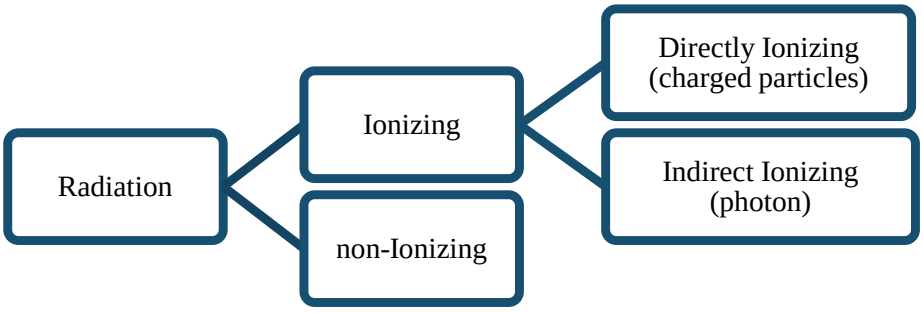

Figure 2.1: Radiation classification [28]

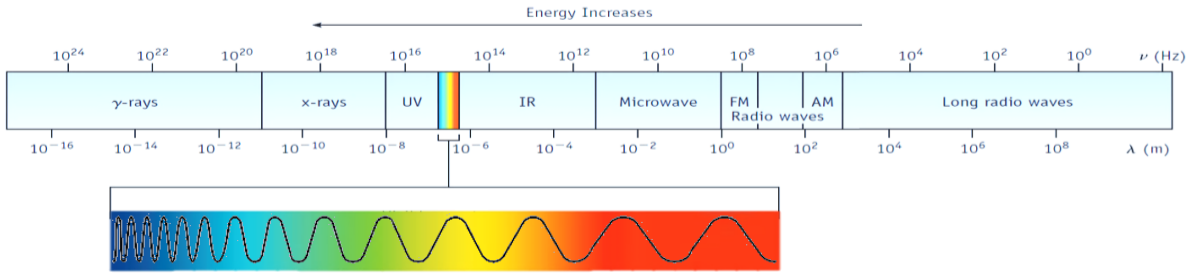

Figure 2.2: Electromagnetic Spectrum [28].

2.2 Photon Radiation Interactions

Gamma ray interact with matter can produce a photoelectric effect, Compton scattering and pair production depending on the radiation energy and the absorbing material.

2.2.1 Photoelectric effect

In the photoelectric effect is an interaction that occurs between the photon and the atomic electron, as shown in Figure 2.3. Typical gamma ray energy is below 1MeV [14].When $\gamma-$ ray hits an atom, the absorbed photon is enough to eject an orbital electron and it is called the photoelectron. The kinetic energy of the generated photoelectron E_K is

$$E_K = E_\gamma - B_e \tag{2.1}$$

where E_γ is the gamma ray energy , B_e is the binding energy of the electron [1, 4]. When the photoelectron is stopped, the output pulse amplitude is proportional to the deposited energy. The probability of this effect to happen is known as the photoelectric cross section or the photoelectric absorption which depends on the atomic number of atom, electron binding energy, and gamma-ray energy [14]. This probablity per unit distance is approximated by the following formula

$$\tau\,(m^{-1}) \cong constant \times \frac{Z^n}{E_\gamma^{3.5}} \tag{2.2}$$

This effect is more probable in lower E_γ and higher Z. This effect is dominant in low $\gamma-$ ray and *x*-ray [4]. The constant term is dimensionless, that does not depend on E_γ and Z.

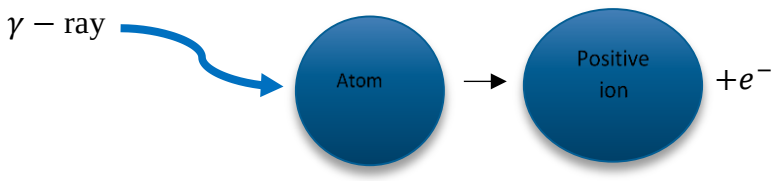

Figure 2.3: The Photoelectric effect [13].

2.2.2 Compton scattering

In this interaction mode, the $\gamma -$ ray collides with a free electron. Since the incident radiation energy (i.e order of keV) is high compared to the binding energy of electron (i.e order of eV), the electron is considered as free electron. The electron and the photon are scattered, as shown in Figure 2.4. Compton scattering is dominant at gamma ray energy below 1MeV [14]. The photon energy is reduced to specific value and is transferred to the electron, and the scattered photon moves in different direction than the incident one with kinetic energy expressed in equation 2.3 and the scattered photon energy is defined in equation 2.4

$$E_K = \frac{\frac{(1-cos\theta)E_\gamma}{mc^2}}{1+\frac{(1-cos\theta)E_\gamma}{mc^2}} \tag{2.3}$$

where is the m electron mass , c speed of the light, θ is the scattering angel of the photon.

$$E_{\gamma'} = \frac{E_\gamma}{1+\frac{(1-cos\theta)E_\gamma}{mc^2}} \tag{2.4}$$

If $\theta = \pi$ this corresponds to the maximum energy of the electron and minimum energy of the scattered photon. The probability per unit distance is

$$\sigma\,(m^{-1}) \cong \rho\frac{N}{2}f(E_\gamma) \tag{2.3}$$

ρ, N are density and the atomic weight, respectively and $f(E_\gamma)$ is function of E_γ. The Compton scattering is independent of the atomic number (Z) [1, 4, 10, 14].

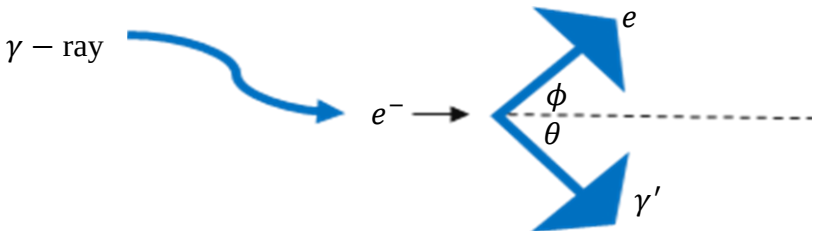

Figure 2.4: Compton Scattering [13]

2.2.3 Pair Production

In the pair production, the interaction occurs between the gamma ray and the nucleus. When the gamma-ray strikes the nucleus, an electron-positron pair is formed, and subsequently two photons are produced when the positron annihilates as shown in Figure 2.5. Typical gamma ray energy is higher than 1MeV [14]. The photon energy is transferred to the electron and positron subtracted by 1.022MeV which is the required energy to produce the two masses. Thus, the kinetic energy of the electron and positron is

$$E_{K,e^-} = E_{K,e^+} = \frac{1}{2}(E_\gamma - 1.022\ MeV) \tag{2.4}$$

The probability for pair production per unit area is

$$\kappa(m^{-1}) \cong NZ^2 f(E_\gamma, Z) \tag{2.5}$$

where $f(E_\gamma, Z)$ is a function of the atomic number and gamma energy. The probability increases with Z and E_γ beyond the threshold value 1.022MeV [1, 4, 10, 14].

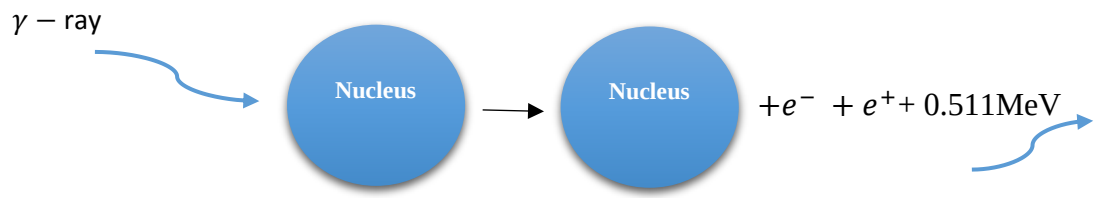

Figure 2.5: The Pair Production [13]

Figure 2.6 shows the relation between *Z* and the energy of the incident photon and the dominant radiation interaction in each energy ranges [4]. For low photon energies up to 0.1MeV, the photoelectric effect is the dominant. The range between 0.1MeV to 10MeV, the Compton scattering is the main interaction. More than 10MeV energy, the pair production is the leading interaction.

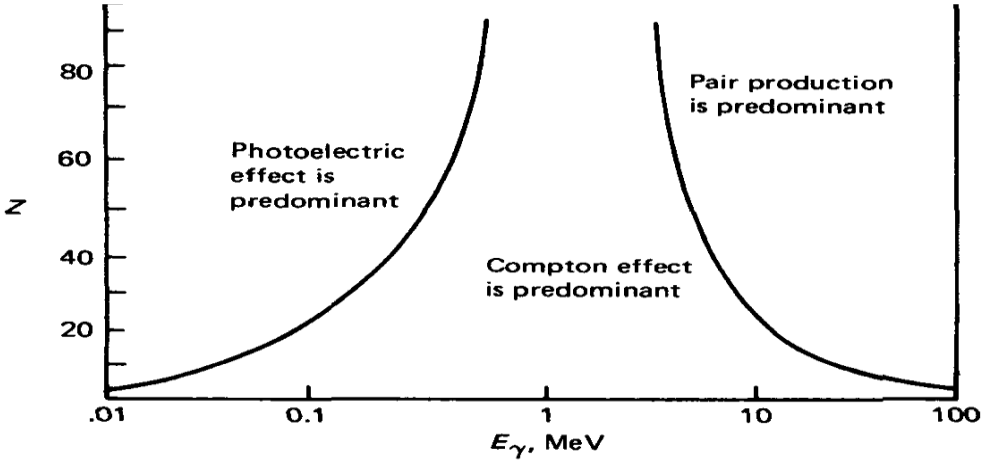

Figure 2.6: The radiation interactions boundary between the Z and E_γ[14]

2.3 Gamma ray Applications and side effects

Gamma ray is used in the medical applications such as medicine, radiation therapy, industry especially in nuclear power, military, scientific researches and consumer products [1, 2, 4]. In the USA, gamma ray imaging is the choice for security applications, in specific, to check the illegal imports [1]. In food production, it eradicates the bacteria and other germs in certain food types. In the industrial radiography, the welded joints in the structure are examined to gamma radiation [2].

Even with these various applications, gamma ray can cause serious side effects and issues.

Since $\gamma -$ ray has high energy, it can cause serious health problems such as cancer. Exposure to $\gamma -$ ray of less than 0.2 Gy dose, (explained later), is sufficient to cause leukemia, thyroid, breast and lung cancers. In addition to the exposed dose, the exposure period (i.e age) is another factor. Children who are exposed to radiation, have high probability of having leukemia, thyroid cancers. Adults have high probability of having lung cancer [2]. Furthermore, studies have reported that the survivors from the atomic bomb show a proportional relation between liver cancer risk and high radiation doses [2]. People exposed to high doses of radiation over short period of time have demonstrated some radiation sickness symptoms such as vomiting, confusion, hair loss and fainting. Also, these rays damage the genes and break the DNA strand. Furthermore issue such as damage and severe skin burns are observed. Therefore, radiation detection is a must and the field of dosimetry is essential field for medical application.

2.4 Importance of Dosimetry

The side effects of the radiation depend on the type of the medium and incident radiation. It is not limited to the human body only, it is powerful to the point it can destroy the materials such as the silicon completely.

Regrettably, there is no clear quantified method to measure the damage that the radiation produces. Disorder in the human cells may not be detected at early stages before it is diagnosed as cancer cells. In addition, the radiation degrades the electronic equipment performance. Despite not providing direct protection, the radiation dosimeters are regarded as vital tools for identifying the presence of ionizing energy, allowing hence for precautionary measures to be implemented on time. Thus, the dosimeters should be able to represent quantitative data or figures that give an indication about quantitative measure for the radiation effect.

2.5 Dosimetry's unit of measurement

To quantify the radiation effects and express measureable values, radiation dosimetry units of measurement are discussed below.

2.5.1 Roentgen

This unit measures the exposure due to gamma rays and *x*-rays and it is based on the amount of ionization that the radiation produces to the air. Typically, 1R is the dose that is required to ionize and produces $2.58 \times 10^{-4} C/kg$ coulombs of negative and positive charges. These charges are produced in one kilogram of air [3, 8].

2.5.2 Absorbed Dose

This term quantifies the amount of energy absorbed per unit mass for any radiation type. The unit is (J/kg) and the SI unit is Gray (Gy). The old unit is *ram*, so $Gy = 100\ ram$. The change of the absorbed dose over a period of time is called absorbed dose rate [8, 9].

2.5.3 Equivalent Dose

The absorbed dose does not provide information about the biological effect of the radiations. Thus, to address such an effect the equivalent dose is introduced. The SI unit is Sievert Sv and the old unit is *rem*, so $Sv = 100 rem$ [8]. In this quantity, there is a dimensionless factor which addresses the different types of tissue [3].

2.5.4 Kerma

It is an acronym of the kinetic energy delivered to the medium per unit mass. The unit is $Kerma$. It gives an approximation for the absorbed dose. It depends on the type of materials that the radiation is exposed to. For example, if the energy is released in the air, it is called $air\ Kerma$[3].

2.6 Existing Technologies for γ-rays detection and dosimetry

In the literature, radiation detectors and dosimeters are classified based on detection mediums (i.e solid, gas, or liquid) in which the ionizing radiation interacts with matter. However, a new classification for the radiation dosimetry is proposed. This classification is based on the collecting mechanisms or what the detector produces as an output after the radiation interactions. In specific, for the heat, light and defect collecting detectors, the change in temperature, the photon production and collecting the defect are the signs of radiation interaction, respectively. In the current collecting detector continuous discharge is the evidence

for radiation interaction. The electron-hole pair production in charge collecting detectors is an indication for radiation interactions. Inspired by having the semiconductor as radiation detector, the memristor is investigated as a potential novel sensor for ionizing electromagnetic, gamma-ray type.

2.6.1 Heat-collecting Radiation Detector (Calorimeter)

Calorimeter is a detector by which the radiation effect can be measured through the change in body temperature during the exposure to ionizing electromagnetic radiation [8, 9]. Many applications employ calorimeters especially in high intensity radiation environments such as radiotherapy [14]. The change in the temperature gives an indication about the absorbed dose. Typically, an absorbed dose of 4180 Gy in water, corresponds to 1℃ increase in the temperature [8].

Calorimeters are classified in three categories which are adiabatic, isothermal and twin cup. This classification is based on the changes in temperature during irradiation. Thus, in the adiabatic calorimeter, the increase in the temperature is translation of detecting the ionizing radiation. Also, there is no heat loss to the outside environment [10]. However, for the second type, the heat is lost to the surrounding and it is equivalent to the heat produced by the ionizing radiation. For the last class, the power generated by the ionizing radiation source is balanced to the generated power in another enclosure from known power source, while keeping the same environment conditions [8]. On the other hand, regardless of the aforementioned categories, the heat loss is unavoidable [8]. To be more specific, since it is insensitive, it requires high amount of radiation exposure in order to have calorimetric measurements [10].

2.6.2 Light-collecting Radiation Detector (Scintillators)

2.6.2.1 Inorganic scintillator

The inorganic crystals consists of an active crystal that can be pure, such as $PbWO_3$ and doped with small amount of impurities, such as Tl in NaI(Tl). The crystal exhibits luminance property when exposed to ionizing radiation. The major application for inorganic scintillator is the detection of high photon energy radiation (i.e gamma rays), since it has high atomic number Z material [11, 19]. The nuclear medicine cameras are made of NaI(Tl) crystals in which the light is detected due to *x*-ray exposure and then it is passed to signal processing unit to reproduce 2D and 3D images [16, 20].

Due to the ionizing radiation exposure on the crystal, an electron moves from the valence band to the conduction band, leaving a hole behind [10, 12, 14-16]. A large number of the generated electron-hole pairs move freely in the lattice and reach the activation centers. Subsequently, electron-hole pairs transform these centers to excited states. The excited states decay to the ground state of the activator center, thus producing the scintillation [12, 15, 17, 18].

The light produced by the scintillator is converted to electrical signal by the photomultiplier tube (PMT). PMT is made of a photosensitive cathode, and an array of dynodes. The cathode releases the photoelectrons [17]. These photoelectrons accelerate under the effect of strong electric field and collide with the dynodes, consequently more electrons are released [16]. Further collisions amplify the charges until they reach the output electrode (anode) and collected [7, 14, 16- 19]. The PMT and the full conversion process is shown in Figure 2.7 [20]

A good scintillator should have a short decay time. For example, the decay time for gamma ray using the NaI(Tl) is 230ns, and 80% of the light intensity is emitted in $1\mu s$ [18, 15, 21]. However, this 1μs response time is quite long for fast timing measurement [13, 14]. Normally, the decay time for the inorganic scintillator is 0.23-4.18 μs and the wavelength of the emission is 415-540 nm [14].

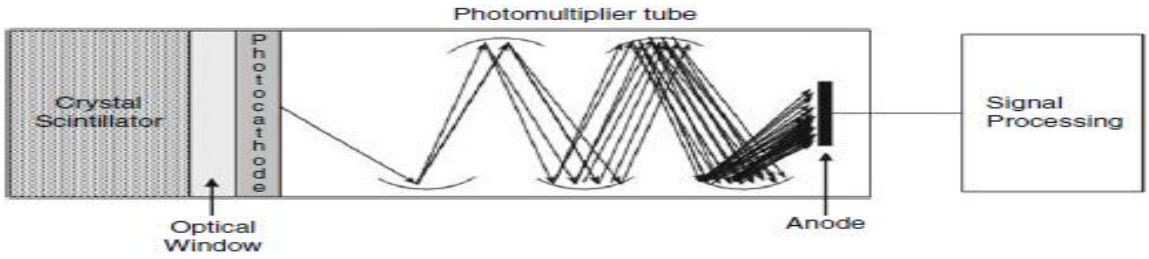

Figure 2.7: Illustration of PMT and the light conversion process to electrical signal [16].

2.6.2.2 Organic scintillator

The organic scintillator is typically made of an aromatic compound such as anthracene, naphthalene and stilbene which poses the luminescence properties allowing to translate the effect of the ionizing radiation [13, 15]. The organic scintillators are used in gamma ray pulse shape discrimination, for environmental studies [13, 19]. The ionizing radiation causes the molecular transitions to a state that is unstable and has high potential energy. Consequently, the molecule decays and this transition emits photon [10, 12, 13-16, 21]. PMT is used to convert the light to electrical signal as in inorganic scintillator [13, 23].

The organic scintillators have much faster response (i.e shorter decay time) compared to inorganic scintillator, specially NaI(Tl). The decay constant is 4.5-30 ns and the wavelength of the emission is 410-447nm [26].

The pros of such a detector is the fast response with less light produced compared to inorganic scintillator [13, 14]. However, some of the organic materials such as trans-stilbene are affected by the thermal and mechanical shocks [17].

2.6.3 Defect-Collecting Radiation Detector

2.6.3.1 Thermoluminescent Dosimeter (TLD)

TLD is kind of memory device that can retain the radiation dose information for long time or after reaching certain threshold temperature [12]. It is used in radiotherapy and has linear response over wide dose ranges [22].

The exposure to ionizing radiation provides sufficient energy to an electron and rises it to the conduction band. However, due to high impurity concentration, the electron falls to an impurity level near the conduction band. After applying a heat, the electron rises again to the conduction band and subsequently, it can fall to the impurities level near the valence band, thus emitting photon. Eventually, the electron falls to the valence band and combines with the hole [12, 13]. The effect of the radiation should be read after radiation exposure. The advantages of such a detector is the recyclability of the TLD materials without sensitivity degradation [14]. One drawback is the low efficiency which around 1% [14]. A detection accuracy between 2%-3% is recorded [22].

2.6.4 Charge-Collecting Radiation Detector

2.6.4.1 Semiconductors

Solids can be classified based on their electrical conductivity into three groups which are conductors, insulators, and semiconductors [12, 13]. Semiconductors are mainly n-type and p-type. These two types are used to form the p-n junction. The depletion region plays an important role in the radiation detection [10, 12, 13-15, 31]. The semiconductor gives the best resolution compared to all spectrometers because of the low statistical fluctuations [14]. It has high charge pair production with linear and fast energy response [12, 33, 22]. It can be designed in special geometry and obtain the best efficiency [13, 18]. One of the disadvantages of the semiconductor as a radiation detector is the high leakage current and noise, thus low signal to noise ratio (SNR) [12].

In the next section the two semiconductors, the silicon and the germanium are well-discussed.

2.6.4.1.1 Silicon based radiation detector

a) Reverse biased p-n junction diode

The depletion region is not enough for radiation detection because of its narrow depletion region depth and large capacitance [12, 14]. To solve this, an external supply of high voltage is applied in which the positive voltage is applied to the n-type region of the p-n junction to assure that the applied potential difference across the junction is the dominant one, shown in Figure 2.8 [12]. [12-15, 19, 29]. As a result, the electric field becomes stronger. Under these conditions, the electron-hole pairs that are produced by the ionized radiation are swept out and this movement will produce an electrical signal that can be recorded for radiation detection [13, 14].

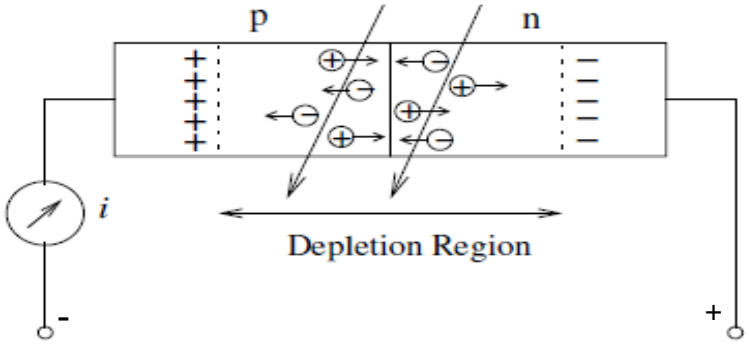

Figure 2.8: Reverse biased P-N junction diode [12]

b) Diffused-junction detector

The diffused-junction detector is designed from thin wafer p-type silicon, as shown in Figure 2.9. It is used to detect the particles. The measurement of the radiation energy is based on the size of the depletion region and the latter depends on two factors which are the impurity concentration and the external applied voltage [14].

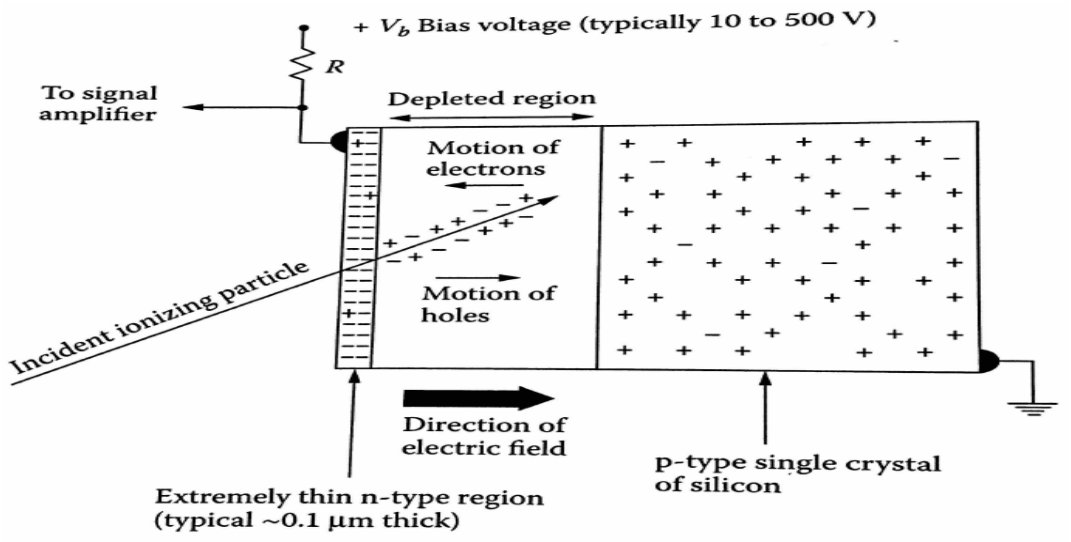

Figure 2.9: Diffused-junction detector [12].

One of the detriments of this detector is the thick dead layer in which the radiation loses part of its energy before reaching the active region and producing the electron-hole pairs. This problem is solved by using the surface-barrier detector, described in the next section.

c) Surface-barrier Detector

The surface-barrier detector, as shown in Figure 2.10, is made of a thin wafer n-type silicon or germanium that is exposed to air for oxidation to form the p-type layer. Consequently, the *p-n* junction is formed [9]. As with diffused-junction detector, the surface-barrier detector is used to detect low energy photons [10, 13, 14, 34]. The detector is made of silicon wafer; it is divided to in two unequal regions. The one with larger width is the depletion region and the other is the dead region. The dead region is small compared to that in the diffused junction detector. It has higher resolution capability compared to diffused-junction detector [9].

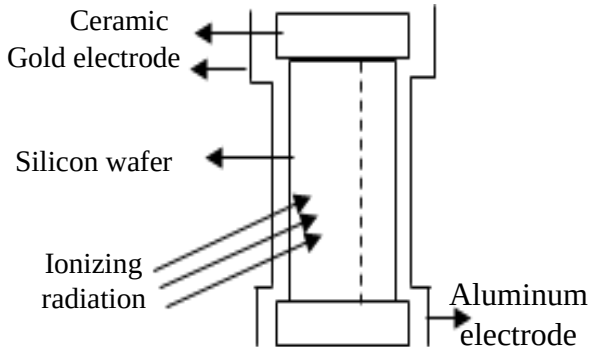

Figure 2.10: The physical structure of the surface-barrier detector [13]

In both surface-barrier and diffused-junction detectors, the sensitivity region is limited to about 2000μm, hence limiting the maximum energy to be detected [12]. For example, the maximum energy for electrons that can be detected is 1.2MeV [13]. Therefore, to increase this energy boundary, the sensitivity region must be increased by diffusing Lithium, Li.

d) PIN diode

In the PIN diode, the depletion region width is the same as the intrinsic region. This region has high resistivity, which means larger width. It is bounded between n-type and p-type layers in order to reduce the leakage current compared to that in the p-n diode [12, 14, 21]. The physical structure and the layer thickness are shown in Figure 2.11. It is employed for x-ray spectroscopy, especially for 1-50keV x-ray energy and, it is the best suited with γ-ray energy below 20keV [18, 19, 34]. The typical resolution is between 140-190eV [34].

The working mechanism is identical to that in P-N reversed bias diode. In which electron-hole pair production is an indication for radiation interaction with matter.

An example of well-known PIN diode detector is silicon(lithium) Si(Li) detector [23, 36]. Introducing the Li will expand the sensitivity region [12, 33].

Figure 2.11: Basic physical structure for PIN diode [14].

All the detectors above function at room temperature, but some applications require the detection at high temperature therefore, SiC is the choice for radiation detection.

e) Silicon carbide detector

The silicon carbide (SiC) detector is considered as substitute to Si at high temperature. It outperforms Si as it has the double the thermal conductivity. This advantage helps in producing high power semiconductor based detector that is thermally stable. The second advantage is that SiC has 8 times Si maximum breakdown field. Consequently, a high bias voltage is applied to improve the charge collection [26]. An example of such a detector is reported in [17], with an energy resolution of 693 eV.

2.6.4.1.2 Germanium based radiation detectors

The germanium (Ge) is another recognized radiation detection material since it has high atomic number. In general, this detector can operate at room temperature because of the low electronic noise [12].

Two common types of Ge detector are discussed next, namely the Li-drifted detector and the highly pure Ge.

a)Germanium Lithium-Drifted Detector

This detector is fabricated same as the Si(Li) detector. The Li is drifted to thin wafer [12, 19]. It can be fabricated into two shapes one is the planar and the other one is the co-axial. The planar type is used for low energy γ-ray and x-ray with efficiency up to about 300keV [19]. Figure 2.12, a, shows its physical design. In the other type, and it is for both γ-ray and x-ray detections with maximum efficiency range up to several MeV. The physical design for this co-axial type is shown in Figure 2.12, b.

The problem of such a detector is the complicated operation which, as a result, limits the production of Si(Li) detector [9]. Hence, the hyperpure germanium (HPGe) is produced.

a)

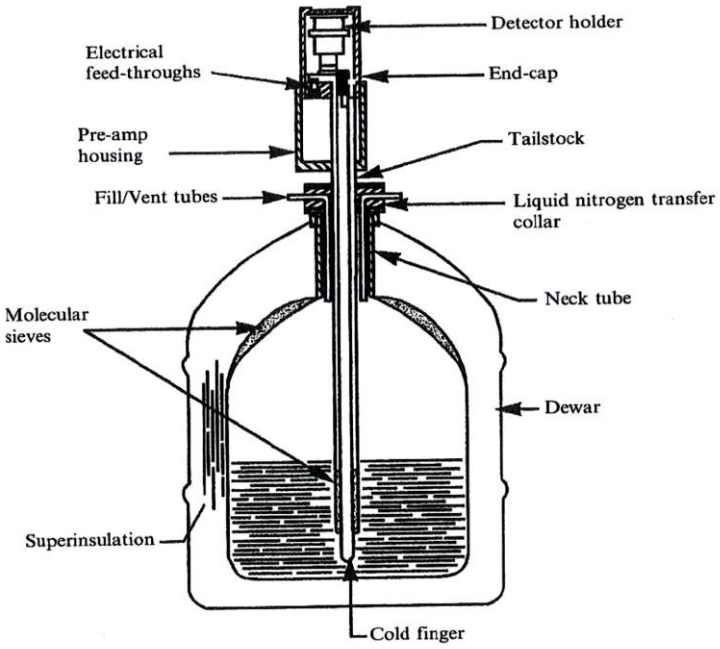

b)

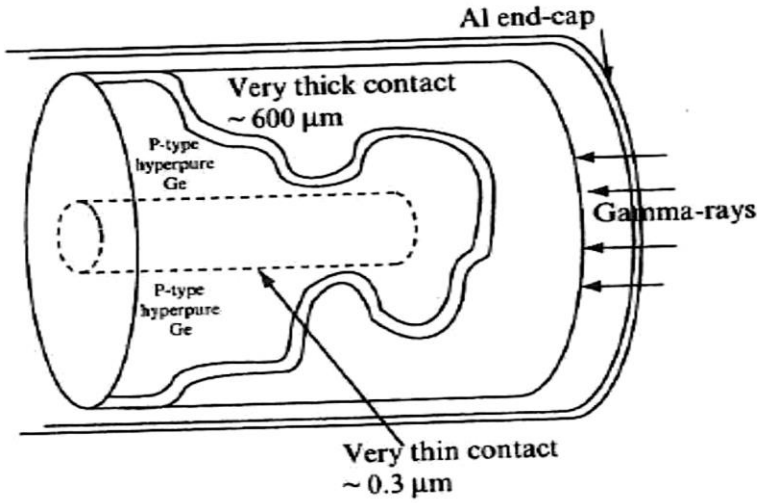

Figure 2.12: The germanium lithium-drifted a) planar shape, b) The Co-axial shape detector [34].

b) High purity Germanium Detector

The fact that Ge can be made in different geometries, facilitates the production of HPGe as the depletion region can be fully utilized [34]. It can be designed into different shapes such as planar or co-axial depending on desired application [18]. The former is made of high-purity p-type Ge [10]. The latter is used for detecting high gamma range energies [18, 37].

The drawbacks are the leakage and the need for a cooling system, to cool the HPGe to 77K. The HPGe has relative efficiency of 150% compared to that in the NaI scintillator exposed to Co photons [12].

2.6.4.1.3 MOSFET radiation detector

The metal oxide semiconductor field effect transistor (MOSFET) is a radiation detector. It is constructed from metal oxide bounded in between silicon substrate and metal gate, as shown in Figure 2.13 [22]. It is used in radiation therapy due to its small size and low cost [20].

The transistor conduction is initiated after certain specific voltage value which is called threshold voltage (V_{th}). The ionizing radiation generates electron-hole within this oxide layer. The electrons move out of the gate electrode leaving the hole trapped in the Si/SiO_2 interface [22, 28]. Consequently, the threshold voltage is shifted to lower level [10, 22, 20]. This deviation is proportional to the radiation dose [24]. P-type is the preferable radiation dosimetry. This is because the radiation damage introduced to Si forms recombination center, which reduces the sensitivity to 1% per kGy and this damage is more dominated in the n-type transistor [18].

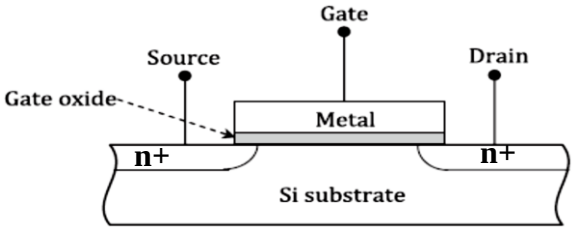

Figure 2.13: Schematic view for nMOS [22].

2.6.4.2 Pulse Ionization chamber

The ionization chamber IC is one of the earliest detectors in which the gas is the medium of detection. It is used in radiation spectroscopy [14]. The ionization chamber can detect gamma rays [8, 34]. It can give information about the physical properties of the charge carriers such as the atomic number and particles charge. Pulse IC are known for its high accuracy in the clinical dosimetry [38].

The voltage operating range is 250-500V that is applied to the anode [10]. It consists of parallel metallic electrodes separated by a distance d and it is filled with noble gas such as argon [12, 15, 26]. The basic parallel plate ionization chamber is shown in Figure 2.14 [14].

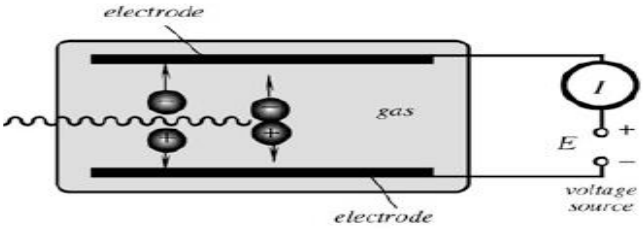

Figure 2.14: Parallel plate ionization chamber [23].

The radiation ionizes the gas, electron and positive ion pairs are produced. Subsequently, these charges are collected at their respective counter electrodes. [12, 8, 15, 34]. The amount of the charges that are collected reflect the physical properties of the incident ionizing radiation [34].

The pulse ionization chamber has high counting rates, up to 10^6 per seconds [8]. Also, since it has high sensitivity, it is capable of measuring the photon energy [14, 34]. Its performance is not affected by the presence of gas contamination [12]. However, sources of electronic noise affect the energy resolution [14]. Its response is subjected to change due to the atmospheric conditions such as pressure [12]. Another drawback is that the pulse amplitude sensitivity to the position of the radiation interactions [14].

2.6.4.3 Proportional Counter

A proportional counter (PC) is a gas filled detector in which it is characterized by the proportionality between the external applied voltage and the output pulse produced. It is employed in the environmental applications. For example, it can be used in monitoring the tritium in the air [28, 34]. As in the pulse IC, the PC is used in the x-ray and γ-ray detections of low energy approximately 100-1000keV and fission fragment detection [18, 21]. The applied voltage is between 500-750V [12, 15]. The physical design is a cylindrical shape in which the anode is a very thin wire of stainless steel (diameter of 0.1mm) [8] and the wall of the counter is the cathode [15]. The gas that is filling between the cathode and the anode is argon [8, 34]. The ionizing radiation produces electron-ion pairs near the anode, where there is high electric field intensity. The electrons and the ions are collected to their respective electrodes and thus providing a correlation with the physical characteristics of the incident ionizing radiation.

2.6.5 Current-Collecting Radiation Detector

2.6.5.1 Geiger-Muller counter

The Geiger-Muller GM is a gas filled radiation detector that needs more than 750V supply voltage to operate [8, 12-15]. GM is the typical choice in many applications in medicine and industry [21, 34]. For example, in the hospitals, the GM is placed near by the radiotherapy treatment rooms to monitor the radiation dose levels [28].

The cathode is made of glass or metal in which the inner wall is metal coated. The gas can be either argon or helium and should be free from the electronegative impurities [4, 8, 30]. The GM tube is sealed and it functions at low pressure levels [34]. GM physical structure is shown in the Figure 2.15.

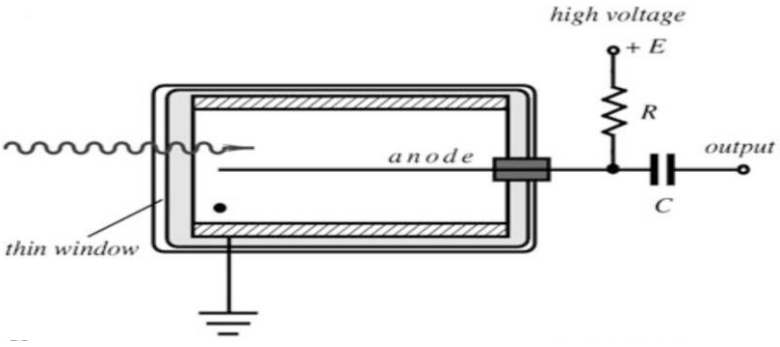

Figure 2.15: GM counter[19]

The basic principle behind the working mechanism of this counter is the maximum amplification [14]. Therefore, the further increase in the operating voltage of the PC produces a stronger electric field around the anode wire. The electrons in this field accelerate and more avalanche is produced and they ionize the gas molecules [12 , 13, 14]. These excited molecules are deexcited to the ground state, so photons are emitted and photoelectrons are produced and collected to their respective electrode [14].

The advantage of such a detector is high amplitude output pulse which reflect the amount of charges that have been collected [12]. It is portable and inexpensive device [12, 13, 24, 39]. Nevertheless, it cannot differentiate between the different types of the incoming particles [14, 34]. GM cannot give any information about the energy of the incident radiation [34].

Figure 2.16, below summarizes the new classification for the radiation detector

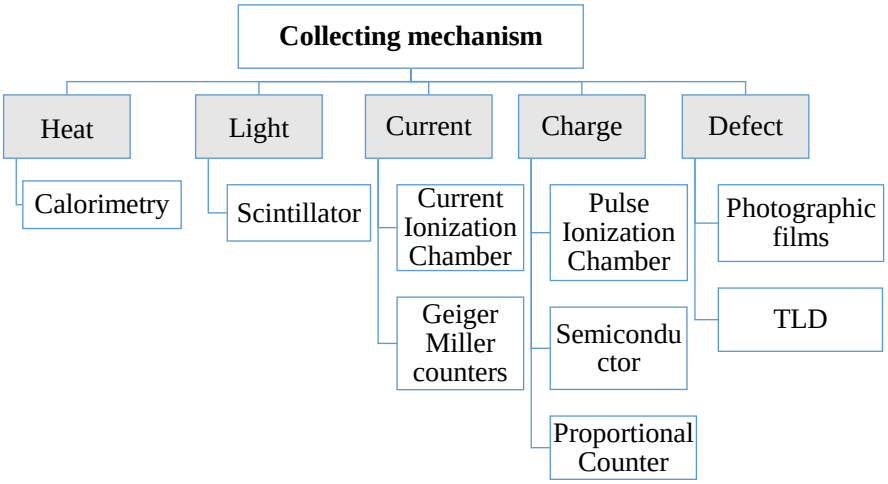

Figure 2.16: Summary of the new classification of the existing radiation detectors based on the collecting mechanisms.

2.7 Emerging technology: Memristor

In 1971, the concept of the memristor was for the first time proposed to the science fields as [41]. In 2008, HP researchers fabricated the first physical memristor [42]. After fabricating the memristor, it is used in various applications such as analog circuits, the biomedical, neuromorphic applications, digital and computing (memristor/CMOS circuits) applications [44, 43]. The memristor is the fourth electrical element which expresses the relationship between the magnetic flux and the electric charge, as shown in Figure 2.17. The name comes from the word memory resistance, thus memristor [46].

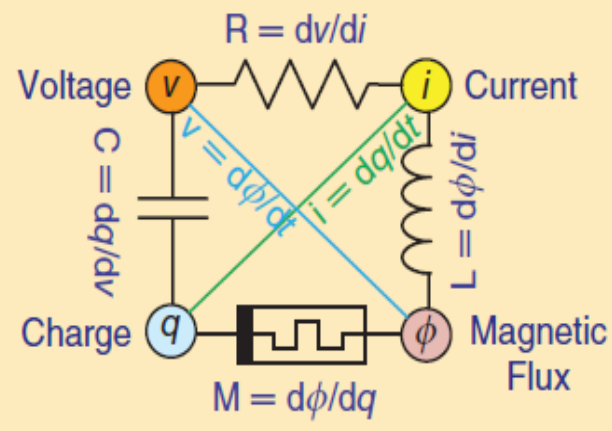

Figure 2.17: The relation between the four electrical fundamental electrical concepts, namely, voltage (V), current (i), charge (q) and the magnetic flux (ϕ)

2.7.1 Switching modes

The memristor has unique I–V characteristics or resistive switching which is hysteresis loop that pinches at zero. The memristor can switch from the low resistive state (LRS) or the ON state to high resistive state (HRS) or OFF state and vice versa. Switching from the LRS to HRS is called RESET process and the required voltage is V_{RESET}, whereas the reverse process is called SET process and the required voltage is V_{SET}. The memristor has two switching modes which are the bipolar and unipolar modes. In the unipolar mode, as in Figure 2.18(a, changing between the two states depends on the applied voltage amplitude only. To reach the SET process, V_{SET} must be greater than V_{RESET}, [45]. The compliance current (CC) in the set switching is essential to avoid the dielectric breakdown [45]. The formation and rupture of the conductive path (nano-width in size) in the oxide layer via joule heating is the reason behind having this switching mechanism. For the bipolar switching, as in Figure 2.18B), the change in the voltage polarity is essential to switch the device ON or OFF [45, 50]. If negative voltage applied to the top electrode, the oxygen vacancies are attracted. The movement of the oxygen anions allow the formation of highly conductive channels under the presence of the strong electric field. In this case, the memristor is ON and it is in LRS. Reversing the polarity of the applied voltage will destroy these channels. Thus, the device will switch OFF or it is in HRS [45].

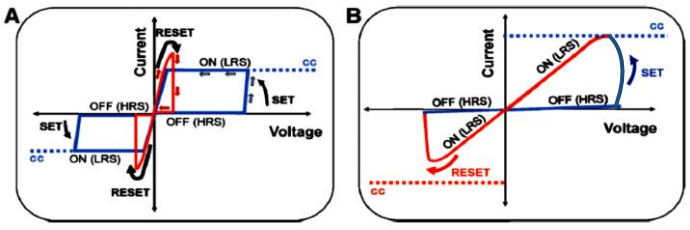

Figure 2.18: The two switching modes: a) unipolar b) bipolar [50]

2.7.2 The physical structure

The memristor physical structure is metal insulator metal (MIM). The thickness for each layer is most commonly in nano-scale range. The physical structure is a cross bar structure which one metal is the top electrode (TE) such as where the voltage is applied and the other one is the bottom electrode (BE) that is grounded. The insulator is metal oxide (MO) material. Typical structure is shown in the Figure 2.19. The insulator is a metal oxide material such as TiO_x, TaO_x HfO_x, TaO_x, MgO, ZnO_x and GeO_x [45]. Recent studies have reported that the memristor can be fabricated at micro-scale thickness [52, 53]

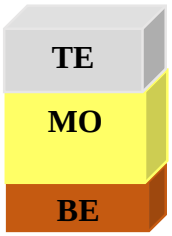

Figure 2.19: Memristor physical structure

2.7.3 Switching mechanisms

One approach to classify the switching behavior is the type of the conductive path. The filamentary conductive path is based on constructing and rupturing the filaments in the oxide material and can be both bipolar and unipolar. In the interface type the switching takes place at the interface between the metal and electrode [45].

Furthermore, the resistive switching of the memristor can be explained based on three switching mechanisms namely, thermochemical change mechanism, TCM, valence change mechanism, VCM, electrochemical change metallization, ECM. The first mechanism is the thermochemical change mechanism (TCM) which can be explained through the change in the oxide stoichiometry behavior because of the rise in the temperature (joule heating) as the current flows [46]. The switching mode is unipolar. Furthermore, the VCM is understand through the oxygen anions drift [45]. The formation and the rupture of the oxygen vacancies filament set, and reset the memristor, respectively. The electric field is the dominate factor that causes the bipolar switching behavior. In addition, ECM is explained cations migration through the solid electrolyte layer. The top electrode is active such as Ag and the bottom electrode is inert such as W [47]. The electric field is the dominant effect for the bipolar switching mode. The different working mechanism is shown in Figure 2.20[54].

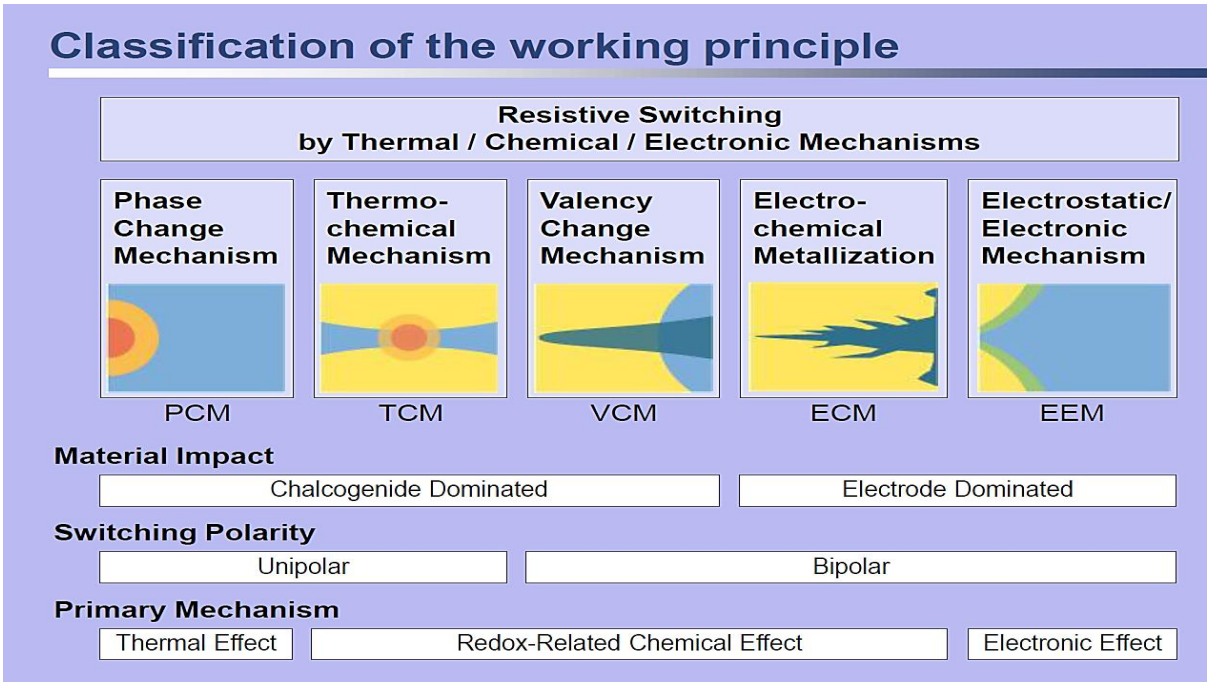

Figure 2.20: The various resistive switching mechanisms for the memristor [54]

2.7.4 Memristor key features

2.7.4.1 Retention

Retention is defined as the ability of the memory to recall the data, over long period of time without the need for power supply [55]. The retention depend on the HRS and LRS characteristics which the latter depends on the size of the conductive filament. The retention is function of the applied CC. Normally, the retention degrades for low CC, because of the weak filaments [55]. In general, nonvolatile memory should have retention time for more than ten years. It should be stable up to 85℃ and small electrical stress of constant stream pulses for the read operation [56].

2.7.4.2 Endurance

Endurance determines the number of the switching cycles in which R_{OFF} and the R_{ON} resistances remain unaltered or slightly varying. It is influenced by device structure, and the read write schemes. Three types of behavior failure are reported and shown in Figure 2.21. One is the loss of the R_{OFF} / R_{ON} ratio, in which R_{OFF} is decreased and R_{ON} is increased due to the formation of the oxide interface during the set process. The second mechanism is the abrupt decrease in the R_{OFF} to the R_{ON} due to the excess generation of the oxygen vacancies because of the strong electric field. The third one is the gradual decrease in the R_{OFF} to R_{ON} value, which is the low rate recombination of the oxygen vacancies, in the electrode layer, so it drops to low resistance state [57].

The endurance is tested by cycling the device within the operating range and then read the R_{OFF} / R_{ON} ratio at low reading voltage.

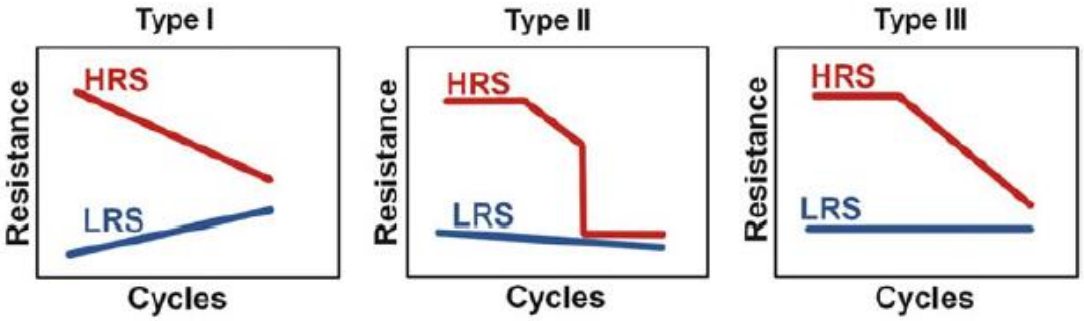

Figure 2.21: Endurance degradation mechanisms [55]

2.8 Gamma radiation attenuation and transmission

When the gamma-radiation incidents on the material, the ionizing radiation attenuates. This attenuation follows an exponential law with constant ratio of the attenuation constant and the density of the absorbing material. The Intensity I_{in} transmitted by the absorber is expressed in exponential expression

$$I_{in=} I_0 \, \mathbf{e^{-\mu_l L}} \qquad (2.8)$$

where I_0 is the gamma ray intensity, μ_l is the linear attenuation constant, L is the absorber thickness. There are four factors which affect the attenuation of the gamma rays radiation while it propagated through the material, which are as the following:

- **Atomic number (Z) effect**

The high atomic number materials interact more with the ionizing radiation than the low Z-material. These atoms present a large target to the radiation, so they impede the radiation movement and the radiation losses part of its energy to the atoms, so affect the absorbing material.

- **Absorber Density**

The high density materials have high probability to interact with matter and it has low transmission probability.

- **Absorber thickness**

Higher thickness corresponds to higher attenuation constant and low transmission probability. The probability of the radiation interaction increases with increasing the thickness of the material.

- **The gamma ray energy effect**

The high gamma ray photon energy means low attenuation constant and high transmission probability, as many materials will be transparent to the radiation [67]

The unique memristor characteristics such as the R_{OFF}/ R_{ON}, the excellent retention, the switching mechanism from HRS to LRS and vice versa can be studied under the irradiation and discovers its sensing capability. Nevertheless, the memristor at the nanoscale has been investigated for its radiation hardness [58-66]. Since the nano-scale thickness, the memristor is transparent to the ionizing radiation. Thus, it is the best suited for space applications. However, the thickness scaling of the active material to micro-scale [52], provides more room for the radiation to attenuate and interact with memristor's material, consequently, influence the switching mechanism.

In the next chapter the electrical characteristics of memristor with and without gamma irradiation is investigated.

Chapter3
Memristor fabrication and Electrical characterization results

In this chapter, the fabrication process of the device is discussed starting from the choice of the material to the final prototype. The electrical characterization results with radiation and without are analyzed

**Please note that, the fabrication was done with other team members, yet the process is described in the coming section for the sake of completeness.*

3.1 Memristor fabrication

3.1.1 Materials selection

The metal oxide is an insulator show sudden switching into the conductive state. It has resistive switching mechanism that changes between the high and the low resistance states [56]. It has simple structure, high density integration, fast switching, low power consumption, low cost and low operating voltage [68-70]. Various examples of metal oxide materials are zinc oxide, nickel oxide and hafnium oxide and Titanium oxide [70]. Among of these oxides, Titanium oxide is well-known material that is used for memristor fabrication as being the insulator or active material that is responsible for the switching mechanism (i.e. VCM). TiO_2 is characterized by its small band gap (E_g) which provides low Ron in the LRS [56, 71]. Also, it has high dielectric constant (K) which will give lower V_{set} , as shown in Figure 3.1[56, 72].

In order to have electrochemical based memristor, the electrode materials should have high ion mobility and ease of oxidation-reduction process [73]. The top electrode namely the anode is an electrochemically active material, such as Ag [70, 72]. The other electrode namely the cathode is an inert or active materials such as W and Cu, respectively [72].

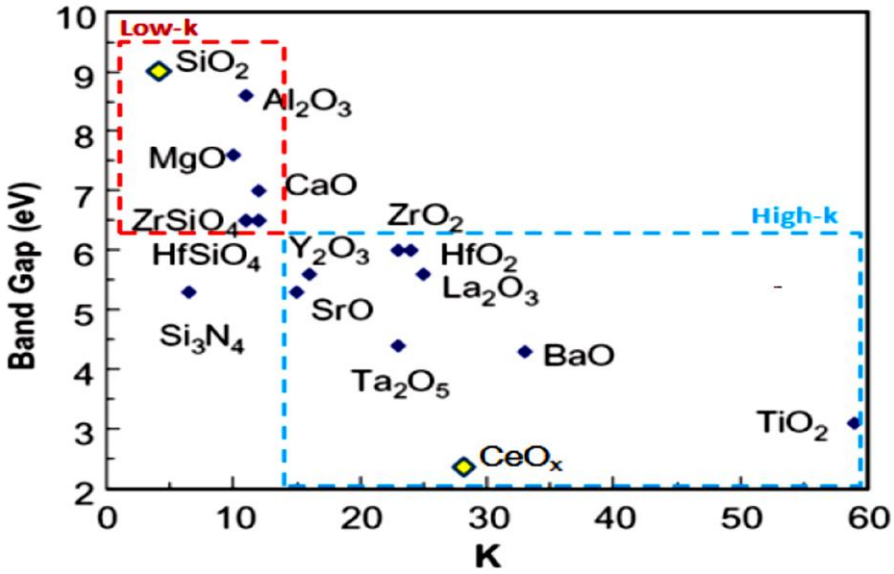

Figure 3.1: Band gap (E_g) versus dielectric constant (K) of different oxide materials [71]

3.1.1.1 Fabrication process

The Fabrication process for the memristor is drop coated Sol-gel. The first thing is to prepare two electrodes of Cu and Ag with 2mm width which will be placed on two plastic substrates. Both plastic substrates are cleaned with ethanol and deionized water. Then, the Ag and Cu are mounted with glue on the plastic substrate. The gluing process should be done carefully so, the glue will come out while gluing the electrode on the plastic. The next step is to prepare the active material. To have this ready, 0.03g of EthylAcetoAcetate (99.9%) and 0.16g TiO_2 precursor (titamium (IV) isopropoxide) 98% which acting as titanium source, are vortexed for 1 minutes using a vortex machine. After that, ammonium acetate (99.6%) is added to make the material in the gelation form. The solution is ready to be added on the electrodes. Thus, using pipette around 3-4 drops are added on the both electrodes and dried at room temperature for 4 days. Then the two plastic plates are glued together in which each electrode is 90°. The active area is 2mm×2mm [74]. The full process is illustrated in Figure 3.2

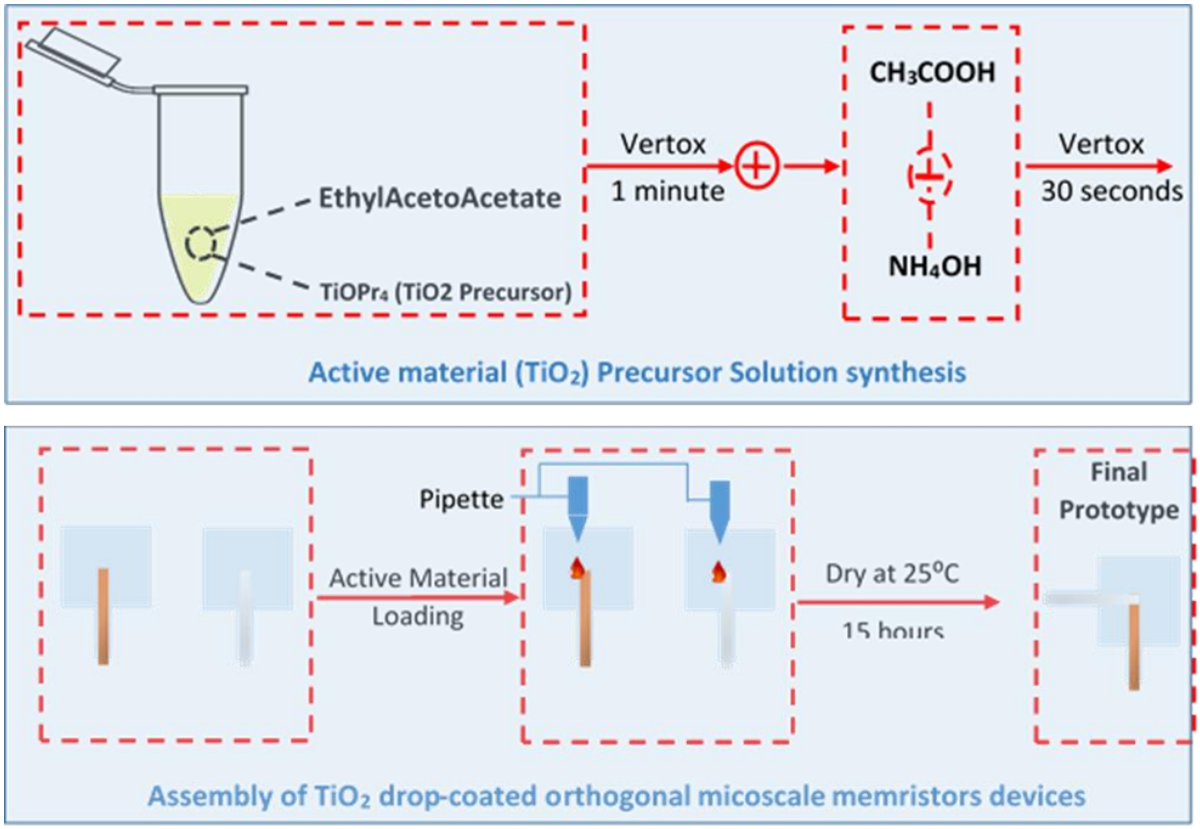

Figure 3.2: Sol gel- Drop coated Fabrication process for Ag/ TiO_2/Cu memristor [74]

The Scan Electron microscopy (SEM) images cross section and the final porotype for the memristor are shown in the Figure 3.3 a, b, respectively.

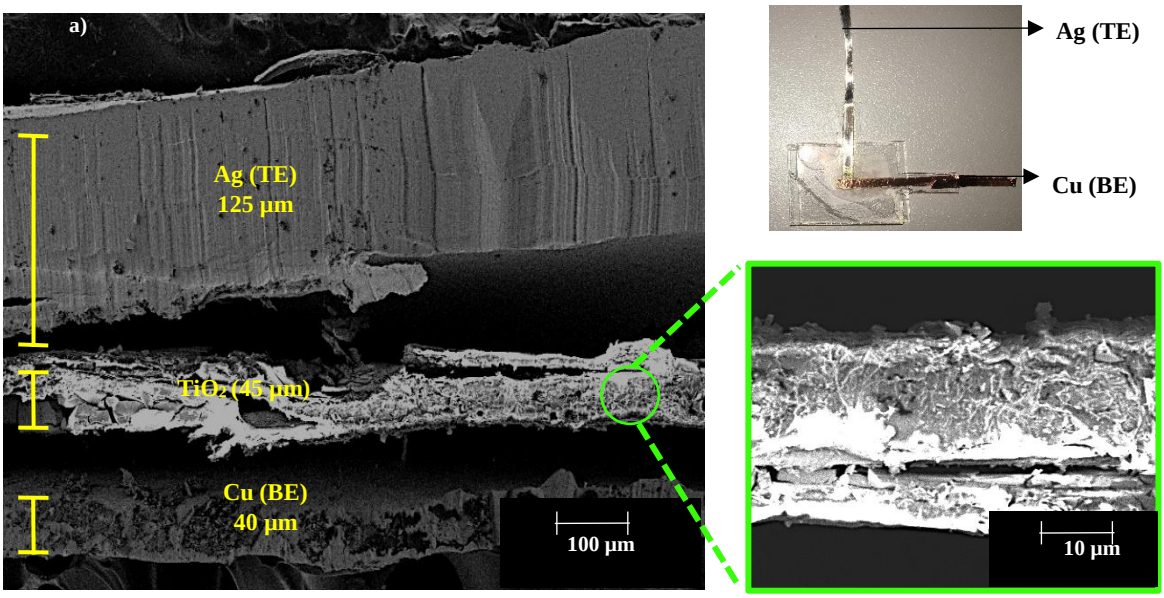

Figure 3.3:a) SEM Cross sectional image of a drop coated Ag/TiO_2/Cu memristors. b) The final physical porotype [74].

3.2 Electrical Characterization Testing and results

The memristor electrical characterization was completed using the Semiconductor characterization system (Kiethley) (SCS) 4200. Different voltage application modes were used such as the voltage sweep and the voltage bias.

3.2.1 Electrical characteristics studies without gamma irradiation

3.2.1.1 I-V characteristics test

Initial scan for the electrical characterization of the device is done by applying, sweep voltage of 5V and CC of 10μA in order to observe the switching behavior in the positive sweep. Then a negative 1V is applied and the CC is removed. After this first screen, if the device did not switch on, further increase in the CC is required, to build strong filament, so it can be ruptured in the negative sweep. The optimal operating range of the memristor is concluded to be a voltage sweep from 1.4 to -0.7 V on the top electrode (i.e Ag). Thus, for the set process, the positive voltage sweep is applied up to 1.4V with 150μA CC and 0.005V/s step size. In this range, the resistance state of the memristor is switched from the HRS to LRS, and this is the set process. The low sweep voltage is intended to reduce any considerable conductance changes. Also, the CC is used to avoid irreversible hard breakdown. To turn off the device, i.e switching from the LRS to HRS, the negative voltage sweep is applied on the Ag electrode and the CC is removed. The resistive switching for the memristor behavior is shown in Figure 3.5. It is pinched hysteresis at zero current and zero voltage indicating no charge storage as in the capacitor. This is bipolar switching mode, in which the set state is sharp switch on, at the voltage V_{set}, is around 0.6V and the V_{reset} is around -0.3V, thus resulting in asymmetric switching. Compared to the Al-Al and Al-Cu micro-thick V_{set} and V_{reset} that are reported in [52, 53], which are $\pm 6V$ and $\pm 0.9V$, respectively, this memristor outperforms all. Also, the writing current for Al-Cu micro-thick is 100mA but for the proposed micro-thick is lower 150μA. This implies that the memristor is of low power for both the set and reset process. Moreover, compared to the reported other nano-scale memristor with Ag /TiO_2(110nm)/Cu (electrodynamic inkjet printing), switches on and off at 0.7V, at -0.7 V, respectively. It requires I_{reset} of 10mA current in the negative sweep to switch off [70]. The proposed memristor operates at low range compared to the aforementioned one.

The switching mechanism is bipolar, sharp with asymmetric switching off and on suggest that the possible switching mechanism is ECM. Initially, the device is off or in HRS and there is no metal electrodeposition on the inert electrode, as shown in Figure 3.4(a).

During the application of the positive voltage at the anode, an anodic dissolution of Ag happens, see Figure 3.4(b), according to the following reaction

$$Ag \rightarrow Ag^{+} + e^{-} \tag{3.1}$$

Due to the presence of the high electric field, the Ag^{+} ions drift across the solid electrolyte (TiO_2) to the other electrode. The ions are reduced on the bottom electrode surface, as shown in Figure 3.4(c), according to cathodic deposition interaction

$$Ag^{+} + e^{-} \rightarrow Ag \tag{3.2}$$

The Ag atoms start to form conductive bridge that grows from the cathode to the anode. The bridge has a low resistance, thus the memristor switches ON, as shown in Figure 3.4(d). The fast switching is due to the high ion mobility and the latter is due to the long-range disorder in the material, thus, the transport paths are fast. For the reset process, the reverse polarity voltage is applied to the Ag electrode. The electrochemical dissolution reset the device to HRS, as shown in Figure 3.4(e) [75-76]. Ag filament is anodically dissolved and the filament is ruptured staring from the Ag electrode/Ag filament interface and this why the reset is abrupt [44]

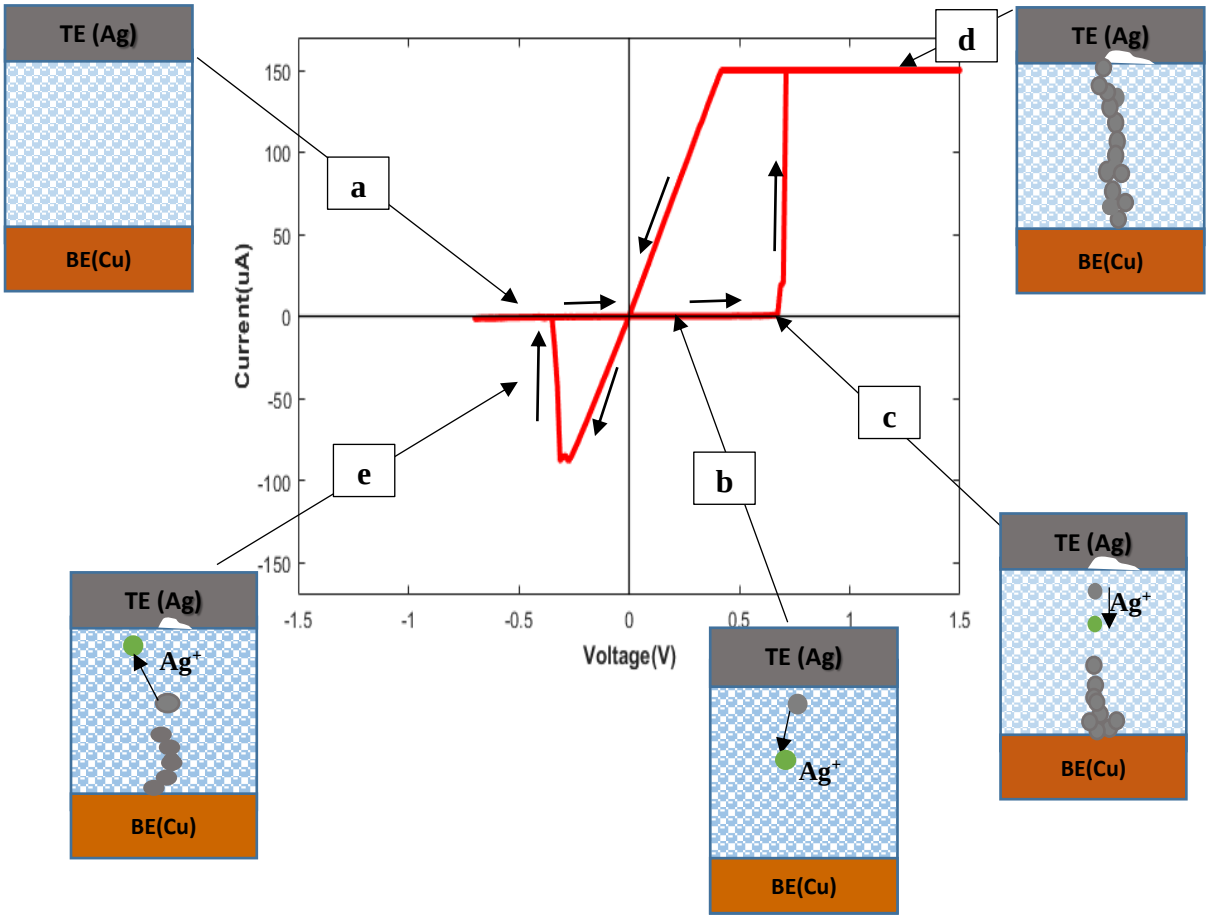

Figure 3.4: Bipolar resistance switching characteristics for Ag/ TiO_2/Cu memristor with CC=150 μA, and voltage sweep -0.7V to 1.4V with the set reset processes.

3.2.1.2 Transient response current in the Set process

The transient response current of the proposed memristor at the set process is shown in Figure 3.5. In this test, the device is switched off, the CC is 150µA and constant positive DC bias voltage are applied at the top electrode. The voltage values are below the V_{set}, (i.e 0.5V), namely, from 0.3V to 0.45V. The device is switched off each time before applying the next DC bias voltage. The time and the current are the variables that are investigated in this test.

It was found that the lower the applied voltage the longer the time required to switch on the device. Any bias voltage higher than 0.3V turns on the memristor in less than 20s. However, at 0.3V or below, it requires more time to switch on the device, in specific, more than 80s. Various factors limit the speed of set process such as the dissolution of the active electrode, the cation migration, the reduction of the ions to metal, and the filament growth. Thus, a possible explanation is the exponential dependence of the set speed (switching time) on the V_{set}, as shown in Figure 3.6 might translate the exponential dependence of the set speed on the electric

field. At voltage values (0.35V and below), the electric field is weak, so the Ag^+ cannot drift as fast as in higher applied voltage. Thus, this requires long time to drive the ions. The slowest process perhaps is the Ag deposition on the bottom electrode. Another explanation is that the new phase formation affects the electro-crystallization rate. As sequence, the growth of the Ag filament is limited [76]. For the range of voltages that are lower than 0.35V, the exponential model does not fit. A possible explanation for this is the 'nucleation overpotential' that must be overcome before any ion migrations to the cathode and initiating the conductive bridge formation. The reverse thing is applied for DC bias values above 0.35V.

This alterations in the switching time, in specific the long time to switch on the device, helps in investigating the radiation sensing at low bias voltage.

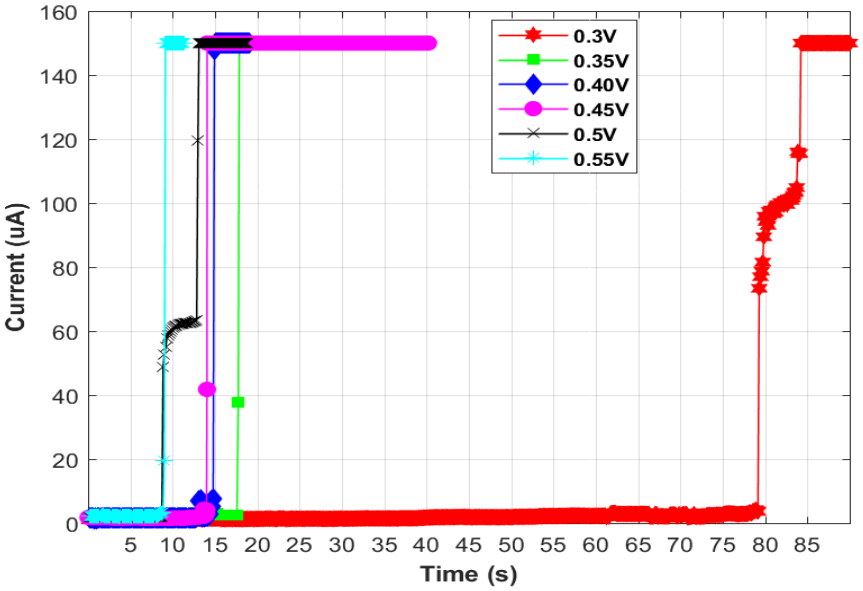

Figure 3.5: The transient response current of the proposed memristor at the Set process at various DC bias voltage

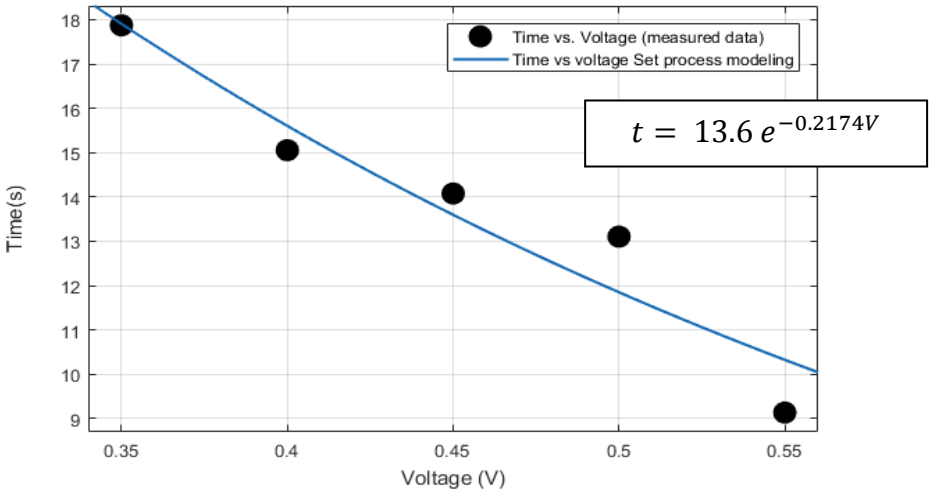

Figure 3.6: The exponential dependence of the set speed on V_{set}

3.2.1.3 Retention test

The retention of the device is investigated for both the LRS and HRS. At the LRS, a positive voltage pulse of 0.1V amplitude and 0.05s pulse width is applied at each 15mintues for 12 hours continuously, at room temperature. At the LRS, the same setting is applicable, however, the voltage is applied with opposite polarity. Figure 3.10 illustrates that both LRS and the HRS resistances are stable for 12 hours ($43200 \approx 10^4\ s$) giving an R_{OFF}/ R_{ON} ratio for more than 10^7. The R_{OFF} is stable, and it is one of feature of the ECM mechanism [60]. The reason behind the good retention is the strong filament at the set process and the good reset at the negative sweep in which the device is switched off completely. The other factor is that the retention depends on the set/ reset algorithms [76]. The CC is factor affecting the set process, so from the protocol applied, the CC is the best to provide long retention. This good retention proposes the memristor for different applications such as logic, memory applications [44] and sensing applications.

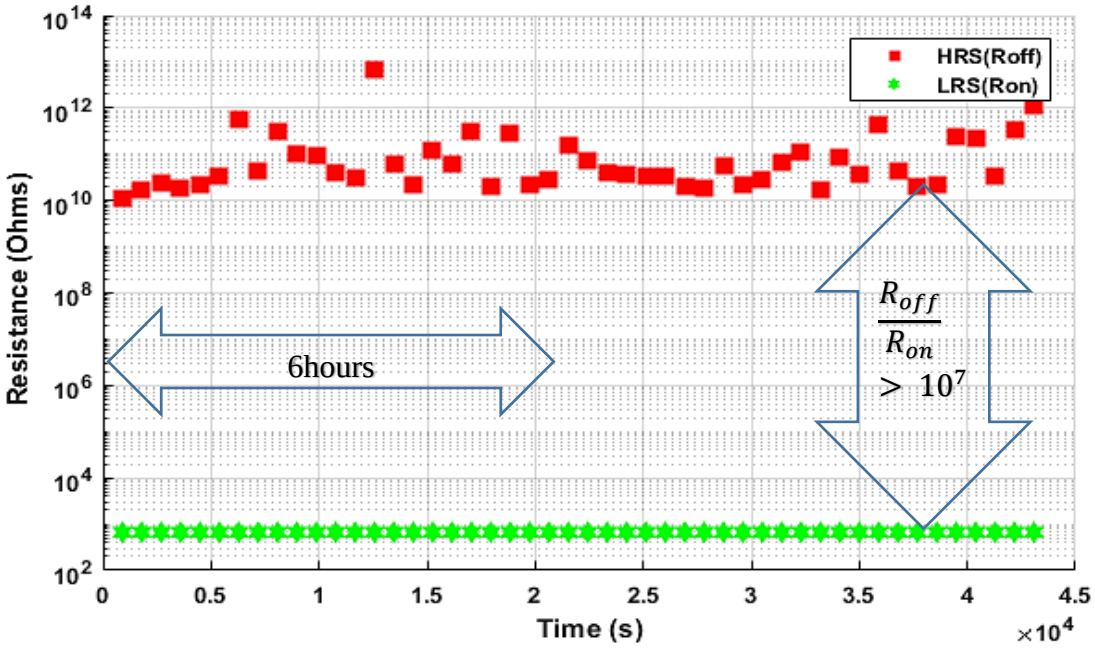

Figure 3.7: Memristor retention characteristics for 12 hours, (semi-log graph)

3.2.1.3.1 Retention modeling:

The HRS is expected to be constant. The LRS can be modeled with exponential modeling in order to predict the retention of the device. The model predicts that after 5 days the R_{ON} increases, as shown in Figure 3.8. This an expected case, for ECM mechanism. LRS is expressed is modelled by the following equation,

$$R_{on} = 666.6\, t^{4.148\times10^{-6}} \qquad (3.4)$$

where the constant prior to the exponent is the R_{ON} after 12 hours and t is the time in *s*. The exponent is slightly higher than zero. This model is the first time to be proposed in the micro-thick memristor, it confirms with what proposed for nano-scale memristor [75]

From this it is expected to have higher R_{ON}, lowering the resistance ratio (R_{OFF}/R_{ON}). Thus, after 5 days, the filament thickness will be reduced and number of the filaments decreases, this will eventually will lead to higher R_{ON} resistance, reaching the OFF state resistance so the device is losing its retention [75].

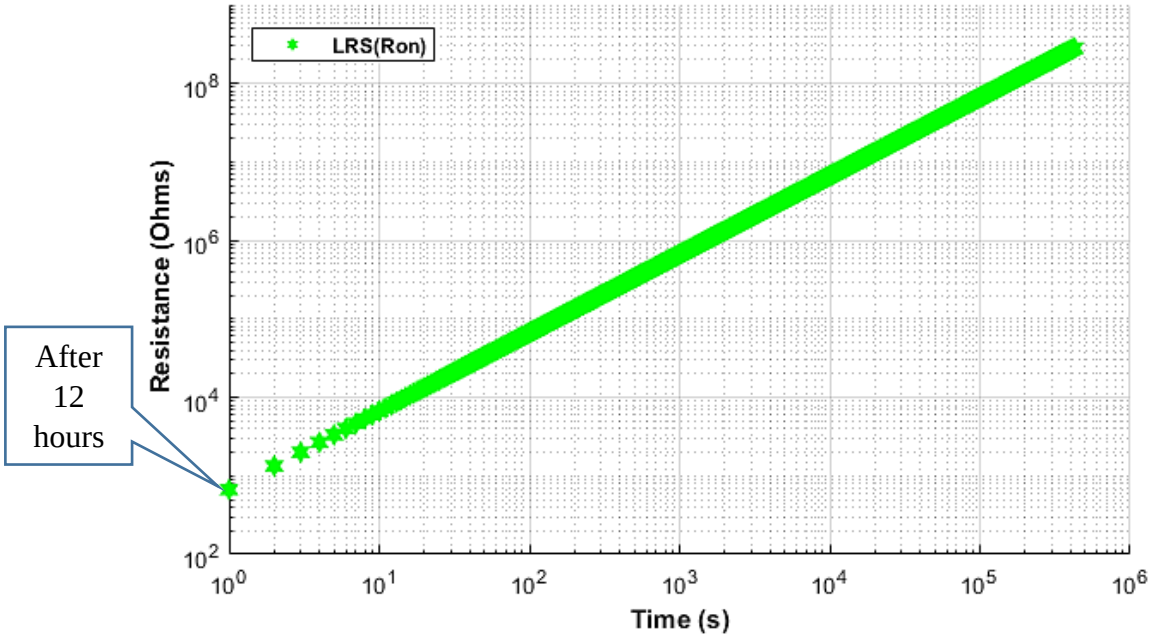

Figure 3.8: The LRS model prediction after 5 days for Ron, log-log scale

3.2.1.4 Endurance test

The endurance of the device have been tested by cycling the device within the voltage operating range which is 1.4V to -0.7V. The device was cycled more than 50 cycles and it has repeatable behavior. Then it cannot be switched off. Figure 3.9 shows the endurance results. The R_{OFF}/R_{ON} is kept the same for the 50 cycles. After the 50 cycles the device could not switch off. This is because the generated electric field is high and the filament could not be ruptured. The low number of cycles compared to what reported in literature can be explained through the manual fabrication process of the device and the extensive cycling for the device. Also, the surrounding environment is playing a role in this test, such as the random noise.

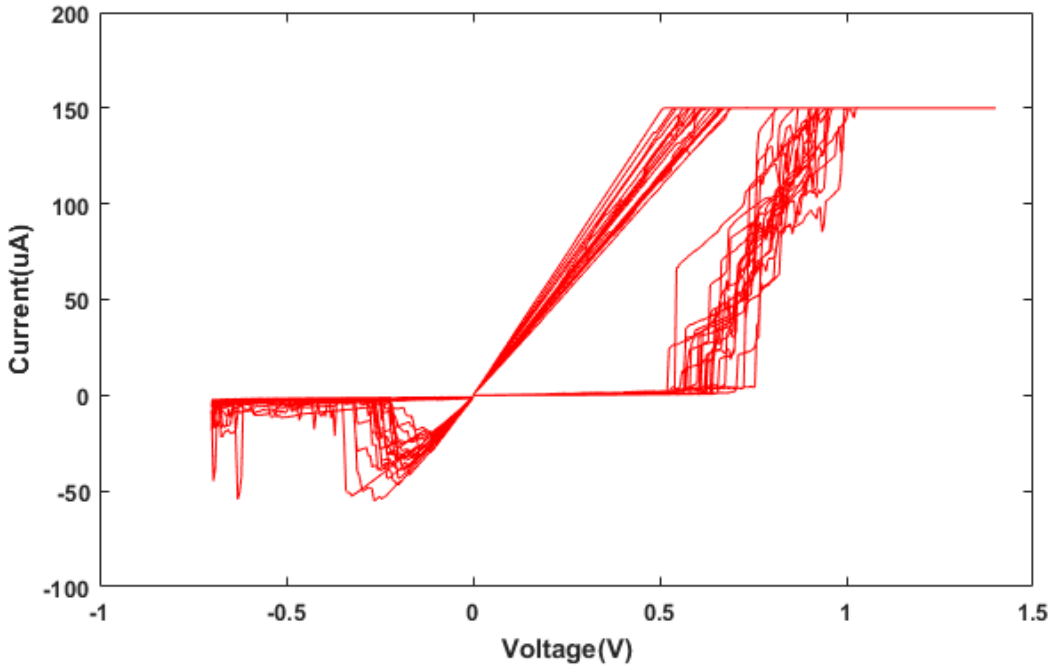

Figure 3.9: Repeatable switching behavior for the proposed memristor indicating the high endurance.

3.2.1.5 Transient response current in the reset process

The transient response current of the proposed memristor at the reset process is shown in Figure 3.10. In this test, the device is switched on for around 20 cycles, the CC is removed and constant negative DC bias voltage are applied on the top electrode. The voltage values are chosen before the V_{reset}. The device is switched on each time before applying the next DC bias voltage. The transient response current of the proposed memristor at the reset process.

The lower the applied voltage, the more time is needed to turn off the device. The reason behind is the local electromechanical redox process near the metal-oxide interface [77]. The oxidation time becomes larger [72]. The Ag filament is ruptured faster in higher applied voltage since there is enough electric field to cause such an event.

Actually, I_{reset} is function of the CC. The higher the CC, the larger the conductive filament diameter, resulting in higher I_{reset}, which requires high V_{reset} [77].

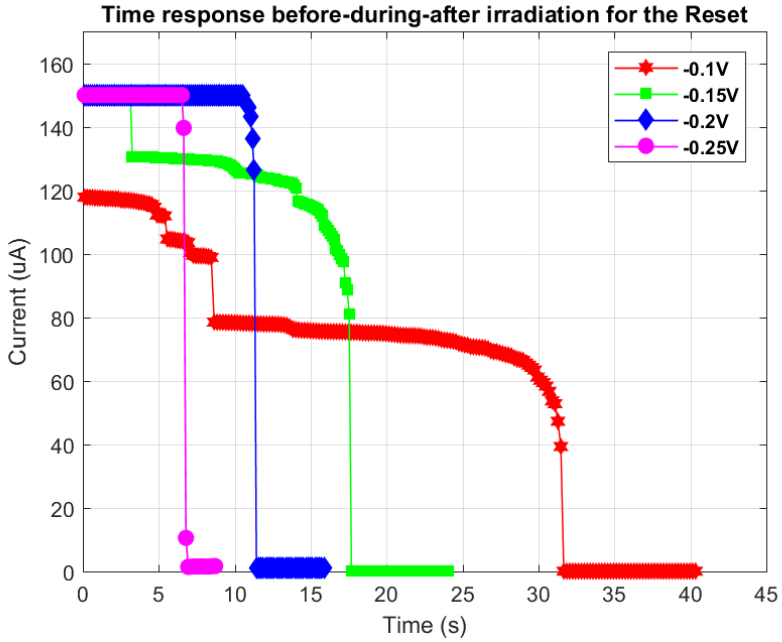

Figure 3.10: The transient response current of the proposed memristor at the Reset process

3.2.1.6 Universal Reset characteristics

The universal reset characteristics of the proposed memristor are analyzed. It has been found that the universal reset characteristics (i.e V_{reset} and I_{reset}) for the bipolar and unipolar devices follow specific trends with the R_{set} [78]. It was reported that V_{reset} decreases linearly with low R_{set} values [78]. Figure 3.11a, and b, study the relation between the V_{reset} versus R_{set} and between the I_{reset} versus R_{set}

For the proposed memristor, V_{reset} varies between 0.2V up to 1V in some devices. The slight increase in the voltage with higher on-state resistance indicates the high R_{reset} and low I_{reset} which means that the filaments are weak and not uniformed well. I_{reset} decreases linearly according to formula

$$I_{reset} = \frac{V_{reset}}{R_{set}} \propto {R_{set}}^{-1} \tag{3.5}$$

The high I_{reset} means both low off state resistance and low on state resistance and higher I_{set} which means the device need lower voltage to switch on. This can be understand in the fact that the filament is not fully off and low current is following inside them, during the application of the positive voltage. Thus, high current levels are following inside the filaments which as result require low reset voltage to turn off.

a)

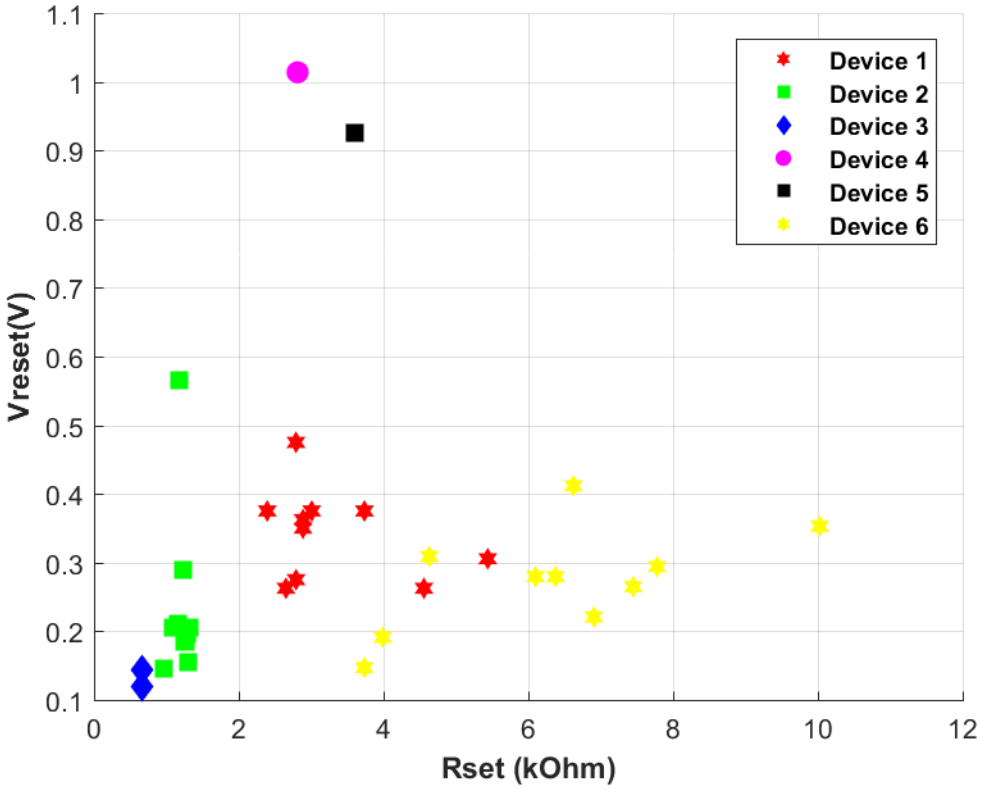

b)

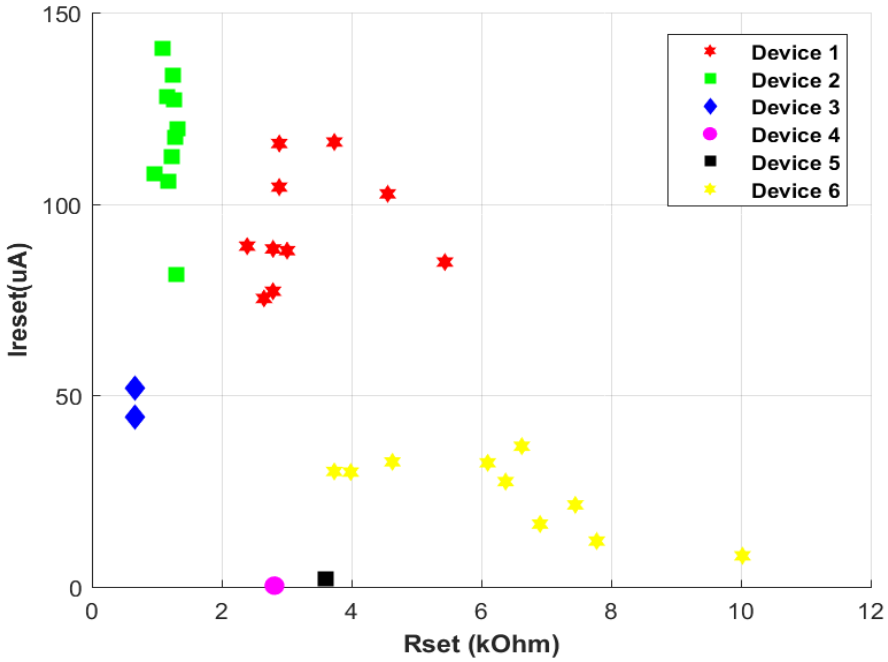

Figure 3.11:a) Vreset and b) Ireset as function of Rset for the bipolar Ag/ TiO_2/ Cu memristor.

3.2.2 Electrical characteristics studies with gamma irradiation

In order to study the memristor as emerging technology for radiation sensing. Various memristor electrical characteristics have been analyzed before during and after ionizing irradiation.

3.2.2.1 Electrical study: I-V characteristics test: before/ during / after irradiation

The I-V characteristics for the memristor is studied by cycling the device 10 cycles, consecutively before irradiation to assure the repeatable response prior to irradiation. The sweep voltage is -0.7V to1.4 V, voltage step is 0.005V and CC=150 μA. The device shows repeatable behavior and no degradation of the off state with high R_{OFF}/R_{ON}. Thus, the radiation sensing property can be investigated. The radiation source is Cesium-137 γ-ray with active diameter of 5mm, type-D, a radioactivity of $5\mu Ci$ and primary emitted photon energy of 662keV. The half-life is 30.07 years. The radiation source is placed directly, in contact with memristor on the plastic substrate facing the Ag electrode for 13mintues. Figure 3.12 a) and b) shows the experimental setup along with radiation source used, respectively. The same cycling conditions are applied for the other two cases which are during and after irradiation cases, as in Figure 3.13 for the three testing cases a)before, b) during, c) after.

Figure 3.12: a) Experimental setup, b) Cesium-137 γ-ray with active diameter of 5mm, type-D, a radioactivity of $5\mu Ci$ and primary emitted photon energy of 662keV

This is bipolar switching mode in which positive polarity is needed to turn on the device and the reverse polarity to turn it off. The radiation lower the dispersion, so it enhances the consistency of the I-V characteristic of the memristor [79, 80], since large amount of Ag ions are generated because the of the gamma ray excitation. The Ag ions drift under strong electric field generated from the carriers induced by the gamma radiation. Table 3.1 provides the

statistical results for the average values over 10 cycles for V_{set}, V_{reset} and I_{reset} with their standard deviations. This slight increase indicates that the device is hard to turn on, as the filament is totally raptured. The device switched off at reverse polarity even during the irradiation. In the presence of irradiation, V_{reset} , I_{reset} and the standard deviations are increasing, but the device returns to its original state after irradiation. This might reflect that there are morphological changes inside the device yet it is not enough to have measurable effects [81]. These variations between during and after irradiation are normal to be recorded for this memristor and are not considered as dramatic changes. This variability comes from the fact that the device has high thickness [82]. Identical conclusions have been reported in Pt (10nm)/ Ta(50nm)/TaO_x (10nm)/ Pt(30nm) memristor that exposed to Co-60 of 1MeV photon energy gamma ionizing radiation [82].

For TaO_x memristor, the reset and the set conditions indicate moderate changes, such as V_{set} is increased from 1.27V to 1.32V, and absolute I_{reset} is reduced form 0.6mA to 0.4 mA, but it is within the range of the device variations and no measurable effect for radiation [83].

Table 3.1: Comparison of the set, reset voltages and reset current memristor I-V characteristics, before, during and after exposure to gamma radiation.

Testing Conditions (irradiation)	**V_{set}(V)** **(average ± SD)**	**V_{reset} (V)** **(average ± SD)**	**|Ireset| (μA)** **(average ± SD)**
Before	0.61±0.04	-0.23±0.12	117.4± 16.78
During	0.64± 0.11	-0.38± 0.19	156.5± 35.36
After	0.73± 0.08	-0.29± 0.05	113.6± 26.96

From the observed I-V characteristics, the effect of the radiation is not clear, further analyses was done at single voltage. This voltage should be lower than any voltage that the device might switch on. This can be confirmed from the set process test that was illustrated in section 3.2.1.2. It was concluded that at 0.3V and lower, the time needed to switch on the device is more than 80s, so the chosen voltage is 0.2V. This time is sufficient to study the effect of the radiation only, without having the bias voltage dominating effect, thus altering the switching mechanism.

a)

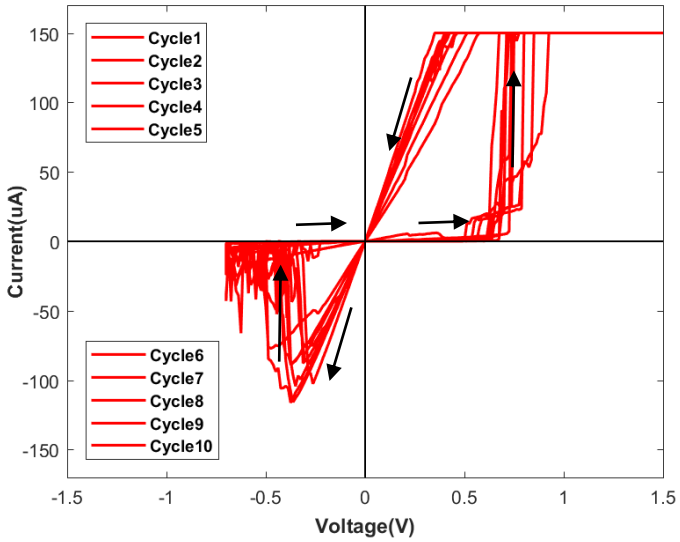

b)

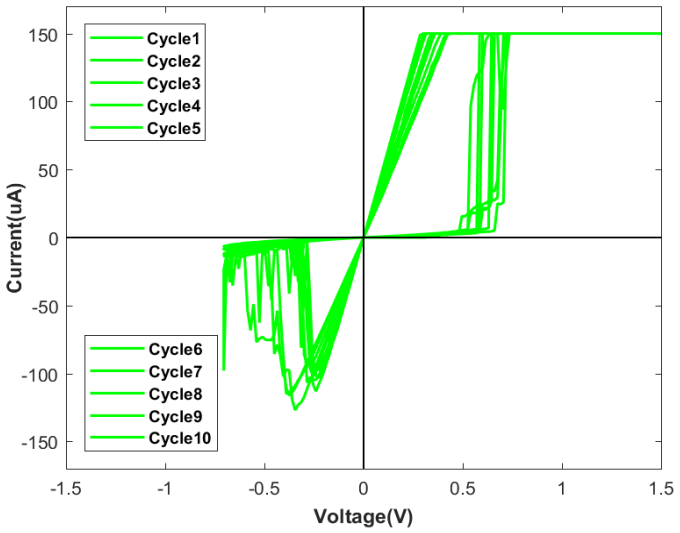

c)

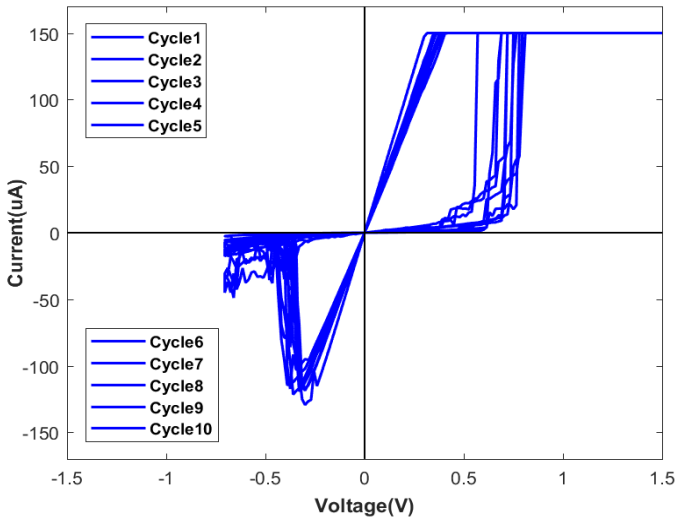

Figure 3.13: Memristor resistive switching before (red), b) during irradiation (green) using Cs-137 662keV γ- ray for 13mintues and after irradiation (blue)

The OFF state current is at 0.2V is shown in Figure 3.14. The OFF state current is the highest after irradiation which it is 1.50 μA, while before and during is 0.48 μA and 0.93 μA, respectively. The high current at 0.2V after irradiation indicates low R_{OFF} compared to other two cases (i.e before and during). The average resistance at 0.2V and the average R_{OFF} for the full OFF state (i.e from 0V and up to V_{set}) for the three testing conditions and it is listed in Table 3.2. It can be concluded that the R_{OFF} deceases after irradiation for both at 0.2V and the full OFF state compared to that for before and during irradiation. The drop in the resistance can be due to the presence of conductive filaments that are not destroyed completely (i.e not fully reset), this can be noticed as well from Figure 3.12 c, so the subsequent switching will be faster, thus resulting in low R_{OFF} after each cycle.

Table 3.2: The average R_{OFF} resistance at 0.2V and the average R_{OFF} for the full OFF state at before, during and after exposure to gamma radiation over 10 cycles.

Testing Conditions (irradiation)	**R_{OFF}($k\Omega$) at 0.2V** (average ± SD)	**R_{OFF}($M\Omega$) at OFF state** (average ± SD)
Before	439.92±116.02	3.37± 0.45
During	217.94± 22.95	3.85± 0.32
After	136.26± 21.00	1.07± 0.14

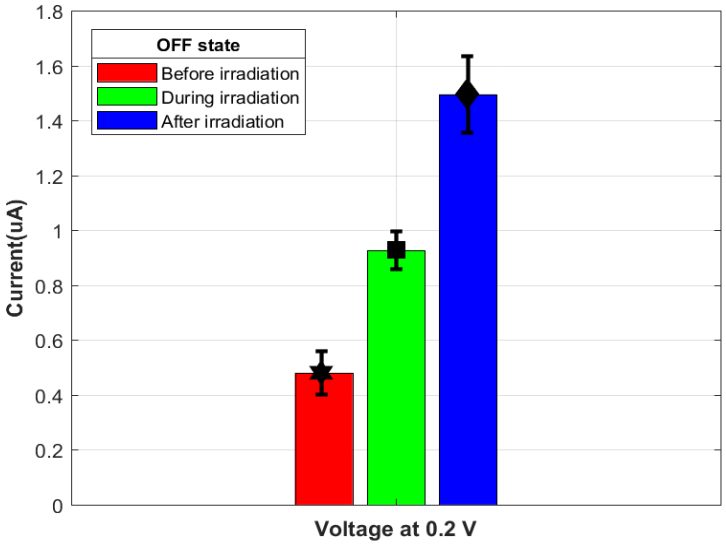

Figure 3.14: The OFF-state current at 0.2V for before, during using Cs-137 662keV γ- ray and after irradiation.

The ON state current is at 0.2V is shown in Figure 3.15. The ON-state current is the lowest after irradiation. The on-state current after irradiation is 114.73 μA, while before and during is 165.87μA and 147.7 μA, respectively. The average R_{ON} at 0.2V and full ON-state, is listed in Table 3.2. Thus, the ON-state resistance for three cases are almost the same. This slight

variations are expected due to the high device variations, and different error measurements (kiethley measurements and averaging errors).

A nano-thick Pt/ TiO_2 /TiO_{2-x} / Pt device was reported in the literature was exposed 1MeV gamma radiation. The R_{ON} did not considerably change after irradiation and the R_{OFF} slightly increased [84]. The constant Ron is due to the similarity in the shape filament during irradiation [84].

Table 3.3: The average R_{ON} resistance at 0.2V and the average R_{ON} for the full on state at before, during and after exposure to gamma radiation over 10 cycles

Testing Conditions (irradiation)	**R_{ON} ($k\Omega$) at 0.2V** **(average ± SD)**	**R_{ON}($k\Omega$) at ON state** **(average ± SD)**
Before	1.21± 0.08	1.3± 0.18
During	1.36± 0.13	1.37± 0.187
After	1.74± 0.25	1.8± 0.24

The resistance ratio R_{OFF}/ R_{ON} drops after irradiation this because the R_{OFF} decrease after irradiation, which is shown in Figure 3.16. This means that the HRS and LRS is not well differentiated. After irradiation the ratio drop from 400 to 100 after irradiation.

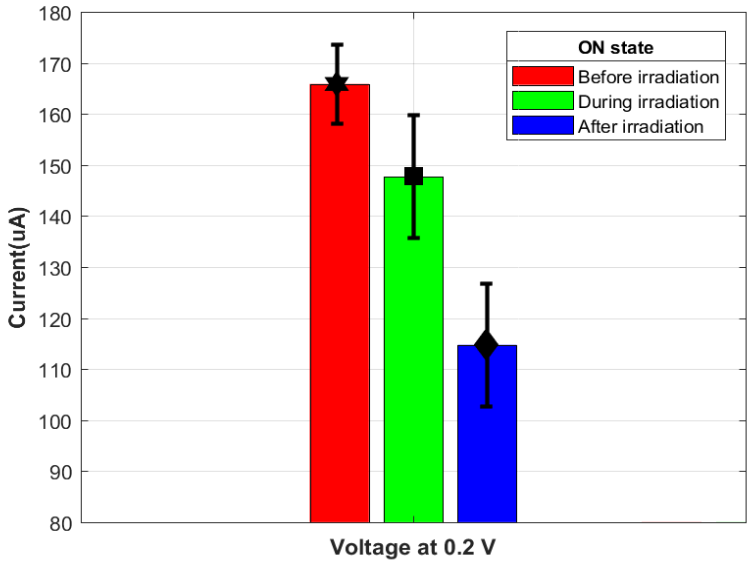

Figure 3.15: The ON-state current at 0.2V for before, during using Cs-137 662keV γ- ray and after irradiation.

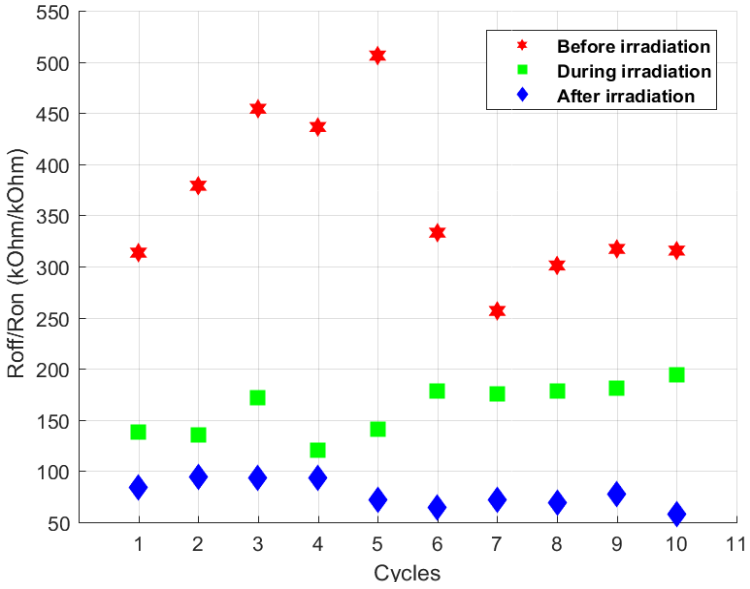

Figure 3.16: The resistance ratio R_{OFF}/ R_{ON} at 0.2V for before, during using Cs-137 662keV γ- ray and after irradiation

Furthermore, the average power during the three cases, at 0.2V is listed in Table 3.4. The total power for both the OFF state after irradiation increased compared to that in during and before irradiation. The P_{OFF} is increaseing as the R_{OFF} is decreasing and this is confirmed with the power-resistance relationship, in which the power is inversely proportional to the resistance. The variations of the P_{ON} match the current variations, while keeping the inverse proportionality. The flucuations are within the device variations and cannot be considered as significan decrease.

Table 3.4: The P_{OFF} and P_{ON} at 0.2V at before, during and after exposure to gamma radiation over 10 cycles.

Testing Conditions (irradiation)	**P_{OFF} (nW) at 0.2V** (average ± SD)	**P_{ON} (μW) at 0.2V** (average ± SD)
Before	96.1± 22.3	33.2± 2.1
During	185.4± 1.99	29.6± 2.7
After	299.0± 39.6	23.0 ± 3.4

Further analyses can done to investigate the power results, is studying the P_{ON} / P_{OFF} and the R_{OFF}/ R_{ON}. The values for the two ratios are illustrated in Table 3.5. It can be confirmed that the two ratios give almost same values with identical standard deviations.

Table 3.5: Comparison between the P_{ON} / P_{OFF} and the R_{OFF}/ R_{ON} at 0.2V for before, during and after exposure to gamma radiation

Testing Conditions (irradiation)	P_{ON} (μW) /P_{OFF} (nW) at 0.2V (average ± SD)	R_{OFF}/ R_{ON} at 0.2V (average ± SD)
Before	345.12 ± 79.80	361.20 ± 79.80
During	159.36 ± 25.09	161.40± 25.09
After	76.75 ± 12.82	77.60± 12.82

During the electroforming stage, several films have been built. Since the device was cycled many times, the following set and reset procedures construct and rupture the filaments at relatively local region (i.e near the electrode interfaces), so the variations in the set and reset voltages are negligible [85].

The number of electrons generated due to gamma radiation is low [82]. This is because the high number of the accumulated induced radiation carriers, which will introduce large field and current. The internally generated field will delay the ions movement. If the effect of polarization is enough, the field reversal can be created and it is high enough to flip the memristor state. Furthermore, due to the high energy of the gamma rays, the radiation induced carrier should be able to produce high current that will set the device to ON-state [84].

Since one of the expected effects due to irradiation is to flip the resistance state, DC bias test has been conducted.

3.2.2.2 The DC bias test

The unique switching mechanism from HRS to LRS is advantage to see if the radiation can induce such a changes inside the device and cause a switching between the two resistance states. The aim is to minimize the effect of any applied voltage on the switching mechanism, but keeping low bias voltage is a must to ensure the presence of an electric field and needed junction for the radiation to produce such an effect. Thus, the challenge in such a test is the proper choice of the voltage bias. This operating voltage value should not cause switching state for sufficient long time. From the set process study that was illustrated in section 3.3.1.2 it was found that the nucleation overpotential is dominant at low voltages. Thus, in order to identify the range for this effect, many voltages value were screened from 0.05 up to 1V. As result, from this screening, the appropriate value for this test was found to be 0.15V.

The memristor is switched off and the 0.15V is applied and the CC is removed. The test is repeated 4 times. The test repeated without and with gamma radiation. The shortest time to see the first jump was 600s (i.e 10mins) and the longest time was 1900s (i.e 32 mins). The current values are fluctuating between 20μA and 50 μA. There were no pattern in which the device switches on, as shown in Figure 3.17, a. Furthermore, the Cs-137 is placed on top of the device. The shortest time to see the first jump was 42s and the longest time was 165s (i.e 2.75mins), as shown in Figure 3.17, b. The current values are fluctuating between 6.5μA and 180 μA. The device switches on randomly with no constant pattern. However, with different trials, the time needed to switch the device on during irradiation is less than the time without irradiation, irrespective of the current values. The fast switching might reflect that the radiation interacts with memristor or it might be within the device variability, since the Cs-137 have high transmission probability due to its high photon energy through the TiO_2. To further confirm the results a radiation source with lower energy than cs-137 is used. Am-241 has gamma-ray photon energy of 60keV. The test repeated without and with radiation. The shortest time to see the first jump was 21s and the longest time was 170s (i.e 2.8 mins). The device switched randomly to different current levels which are between 5.5 μA and 13 μA, as shown in Figure 3.15, c.

Memristor under Am-241 irradiation switches on faster and at lower current levels compared to that without irradiation case. However, there is an overlap between the time instants and the currents between the Cs-137 and the Am-241. However, generally speaking, the memristor during Cs-137 irradiation switches on faster with higher current levels than during the Am-241irradiation. A possible explanation is that the exposure to high energy irradiation (i.e Cs-137 in this case), accelerates the oxidation and the drift of Ag ions becomes faster, thus allowing the fast filament formation. However, the variations in the current levels without constant sequence might indicate that the device is highly random and there no effect for the gamma radiation.

The results from the previous testing could indicate that the radiation interacts with memristor. However, during the forming stage, several ions films have been constructed. Since the device was cycled many times, the subsequent set and reset, constructs and ruptures the filaments at relatively local region (i.e near the electrode interfaces), so the variations in the set and reset voltages are negligible [83].

Cs-137 with gamma ray of 662keV is likely to have the Compton scattering effect on TiO_2 . It might be that the number of electrons generated due to gamma radiation is low since it is thin

film (i.e small thickness) [85]. Thus, the electrons and the photon scattered quickly without introducing an effect in the memristor.

The number of induced radiation carriers can generate the current or field affect the device performance. They accumulate near the oxide/metal contacts, and the locally generated field within the device impedes the ions movement, thus, there will be no effect for the gamma radiation. The DC bias test indicates that the device might switches on at shorter time compared to the case without irradiation. Nevertheless, the results cannot be generalized until repeatable results can be produced.

In the literature, it was reported that SiO_2(200nm)/ Pt(10nm) / Ti(5nm)/TiO_2 (26nm)/ Pt(10nm) device was exposed to 1MeV γ-ray, shows no effect for irradiation because the gamma ray have high transmission probability and the secondary electrons that ionize the sample, travel away from the TiO_2 thin films [85]. The proposed memristor gives similar results.

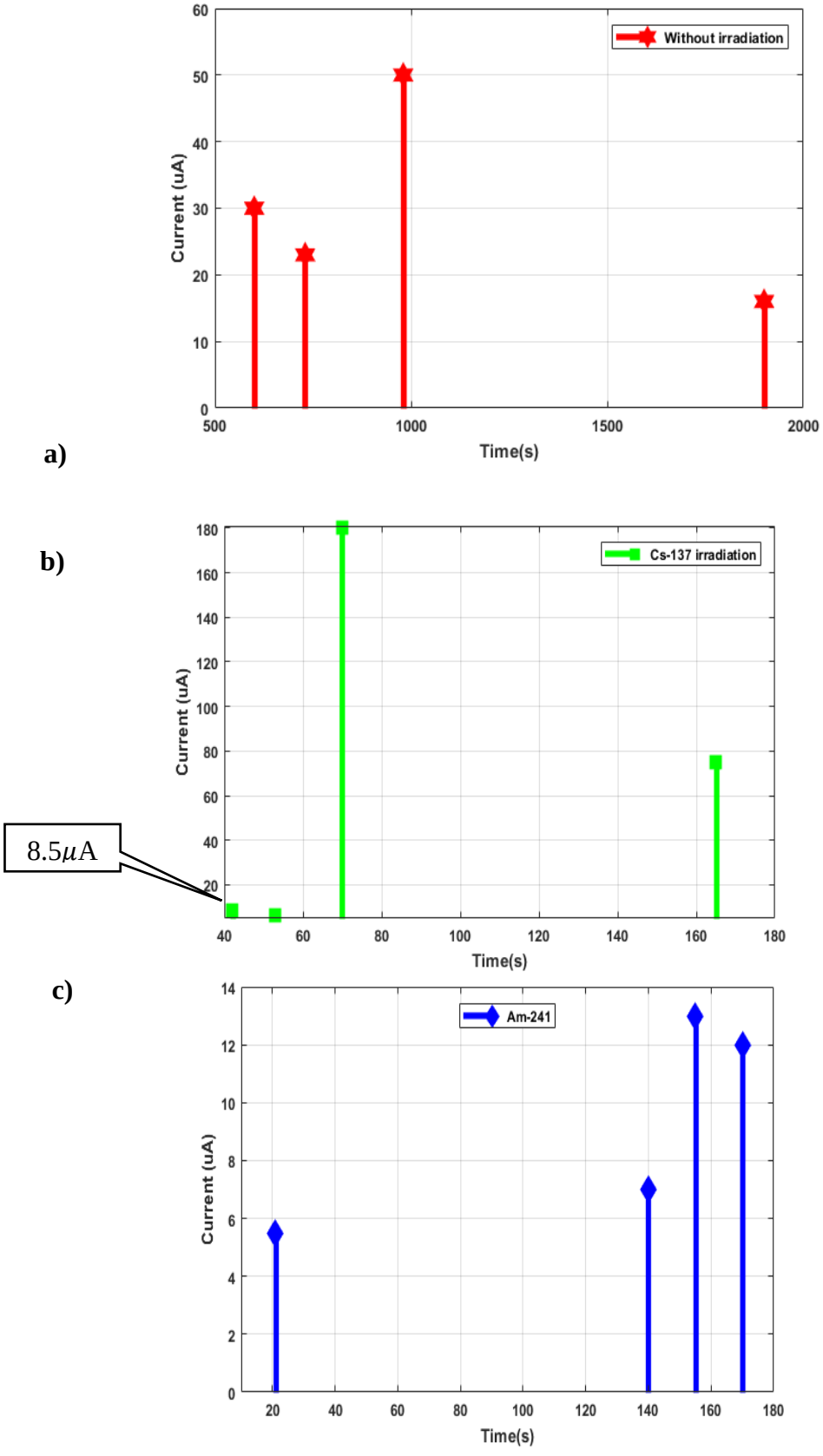

Figure 3.17: DC bias test at 0.15V: a) without, b) Cs-137 662keV γ- ray, c) Am-214 60keV γ- ray irradiation

In the next section, nuclear experiments were implemented to further confirm the radiation effect.

3.2.2.3 Nuclear study: Nuclear calculations and experiments

In order to verify the electrical characterization results, the attenuation constant was studied and some nuclear experiment was done in the nuclear lab, on experiment is presented here and the other is attached in Appendix B

3.2.2.3.1 Attenuation constant calculations

As stated earlier, gamma rays attenuated while propagating inside the material. The Linear attenuation constantμ_l for gamma rays determine the minimum thickness that the gamma rays in order to interact with absorbing material. The reciprocal of the linear attenuation constantμ_l is the mean-free path (L), which is the average thickness a gamma ray requires to travel in the absorber before interacting with the matter. For the proposed memristor, the radiation faces the Ag electrode and TiO_2. The radiation should at least interacts with one of the materials to have effect on the memristor. The following calculations are for the mean-free paths for the Ag and TiO_2. Thus, for Ag it was reported in [87], that $\mu_{l_{Ag}}$ for the Cs-137 gamma ray is 0.137 cm^{-1}.

$$L = 1/\mu_{l_{Ag}} = 1/0.137\ cm^{-1} = 7.3cm \quad (3.5)$$

Thus, the Ag mean free-path or the minimum thickness the energy interacts with Ag is 7.3 cm. The μ_l for the compound material is calculated from the product of the material density (ρ) with its mass attenuation constantμ. The latter is calculated for each element in the compound as the following formula

$$\sum \mu_i w_i \quad (3.6)$$

μ_i is the mass attenuation constant for the i^{th} element and the w_i is the weight fraction of the element. For the TiO_2, the chemical formula for the solution used in the fabrication is $C_{12}H_{28}O_4Ti$. Considering C and H as defect we have to calculate the w_i and μ_i for Ti and oxygen. w_i and μ_i for Ti and oxygen are summarized in Table 3.6. It is worth mentioning that for μ_i, there are graphs of $\mu_i$versus the photon energy used for irradiation which is available in the literature as [88]

Table 3.6: μ_i and w_i for both the Ti and oxygen

Material elements	$\boldsymbol{\mu_i}$ (cm^2/g)	$\boldsymbol{w_i}$
Ti	7.529×10^{-2}	0.428
oxygen	8.070×10^{-2}	0.572

Thus, the total $\boldsymbol{\mu}$ is

$$\mu = \mu_{Ti} w_{Ti} + \mu_O w_O = 0.07838 \quad (3.7)$$

The ρ for TiO_2 is provided by the supplier which is 1.033g/ cm^3

The mean free-path for TiO_2 is

$$L_{TiO2} = 1/\mu_l = 12.35 \text{ cm} \quad (3.8)$$

The gamma radiation with photon energy of 662keV requires 12.35cm to propagate through the material to interact with TiO_2 only. Therefore, for the memristor stack of Ag and TiO_2 , it is required to have the mean free-path as the following

$$L_{mem} = L_{Ag} + L_{TiO2} = 7.3 + 12.35 = 19.65 \text{cm} \quad (3.9)$$

From the calculations above, the low thickness of the memristor is one of the reasons why the effect of the irradiation might not be measurable.

3.2.2.3.2 NaI and the radiation source gamma ray spectrum.

To further confirm the results from the previous experiment, the NaI scintillator detector is used. The detector is connected to PCI Card software in which the counts versus the photon energy is generated. The radiation source is placed inside the detector without the memristor. The next step is to place the memristor on top of the radiation source for both Cs-137 and Am-241, individually. The graphs for both stages are identical, as shown in Figures 3.18 respectively. The results confirm that the high transmission probability for the gamma rays through TiO_2, so the radiation propagates very fast through the memristor without depositing sufficient energy that affects the switching mechanism. In addition, the Am-241 is used in this study and it shows that the memristor is transparent for the radiation even with photon energy of 60keV, as shown in Figures 3.19 a) and b) for both the Am-241 radiation source only and with memristor and the radiation source.

a)

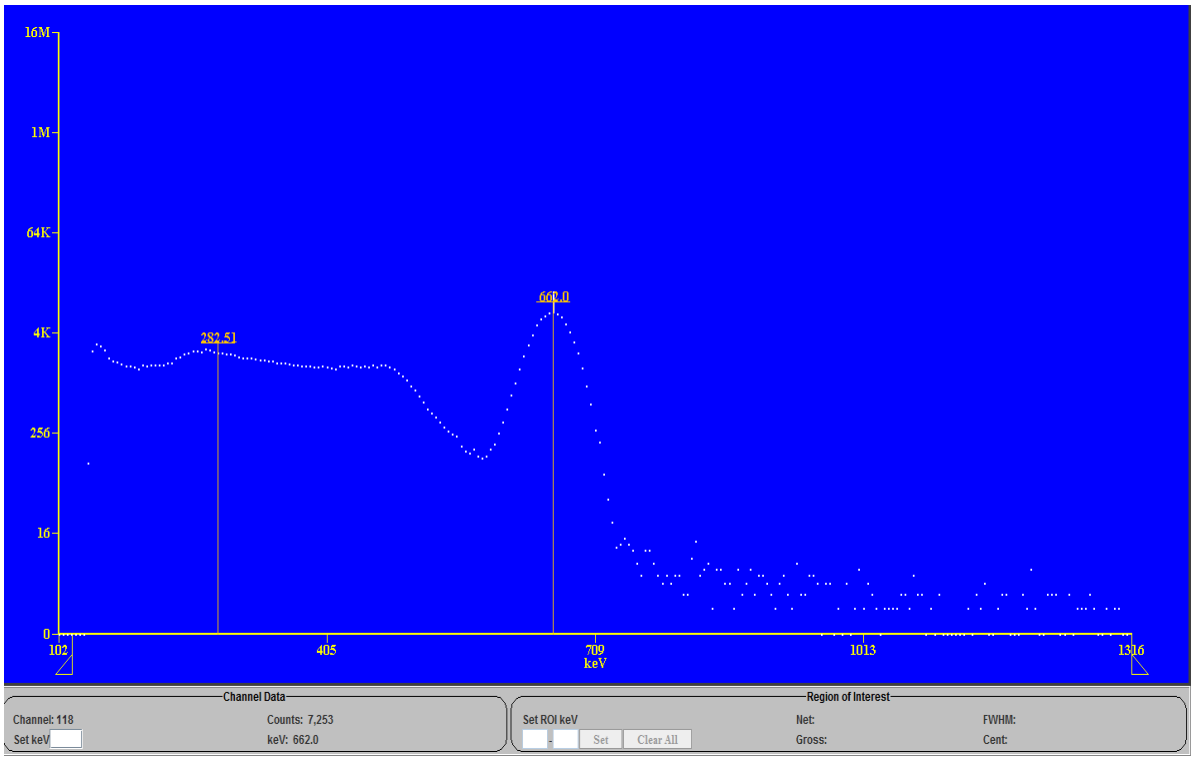

b)

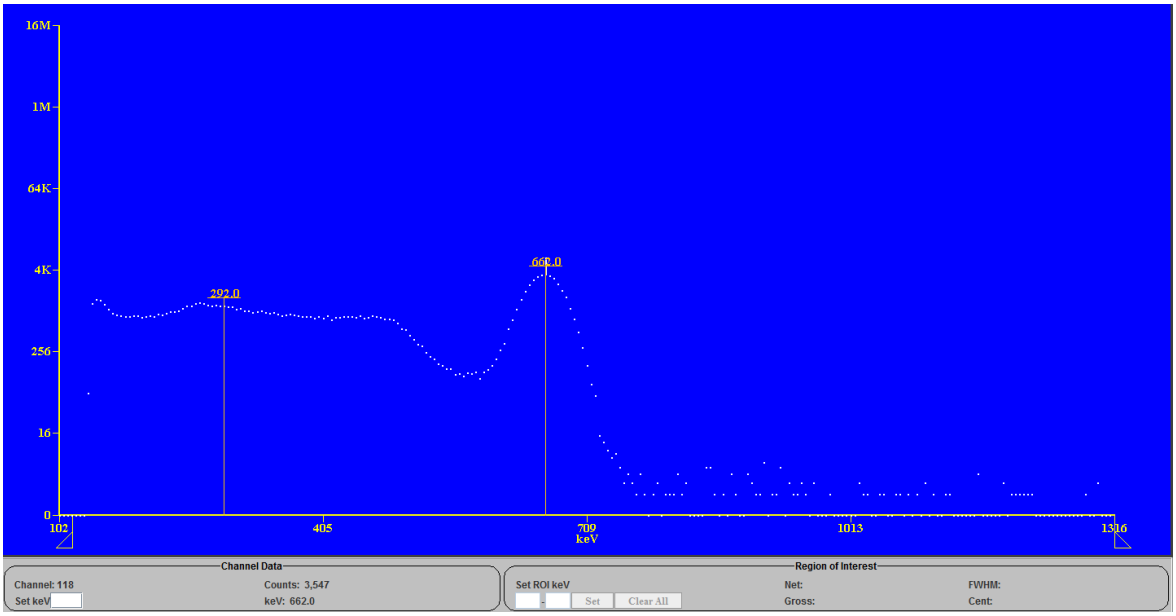

Figure 3.18: The photon spectrum for gamma rays,a) from Cs-137 only,b) passing through the memristor from Cs-137

a)

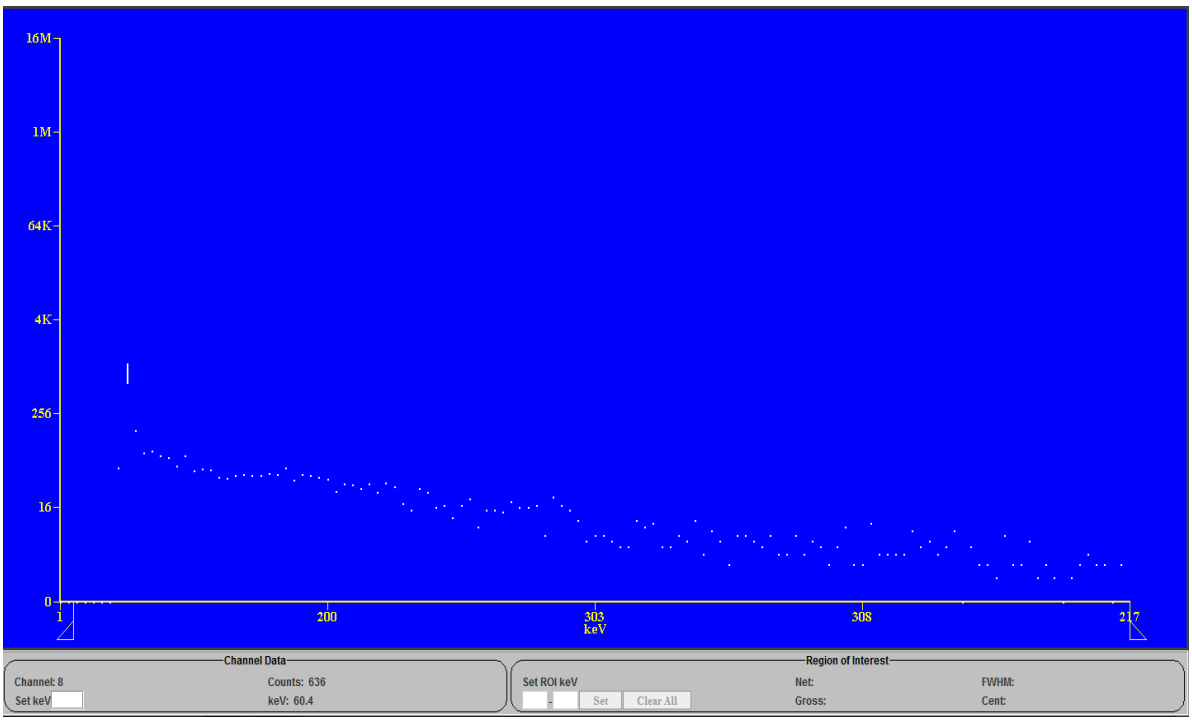

b)

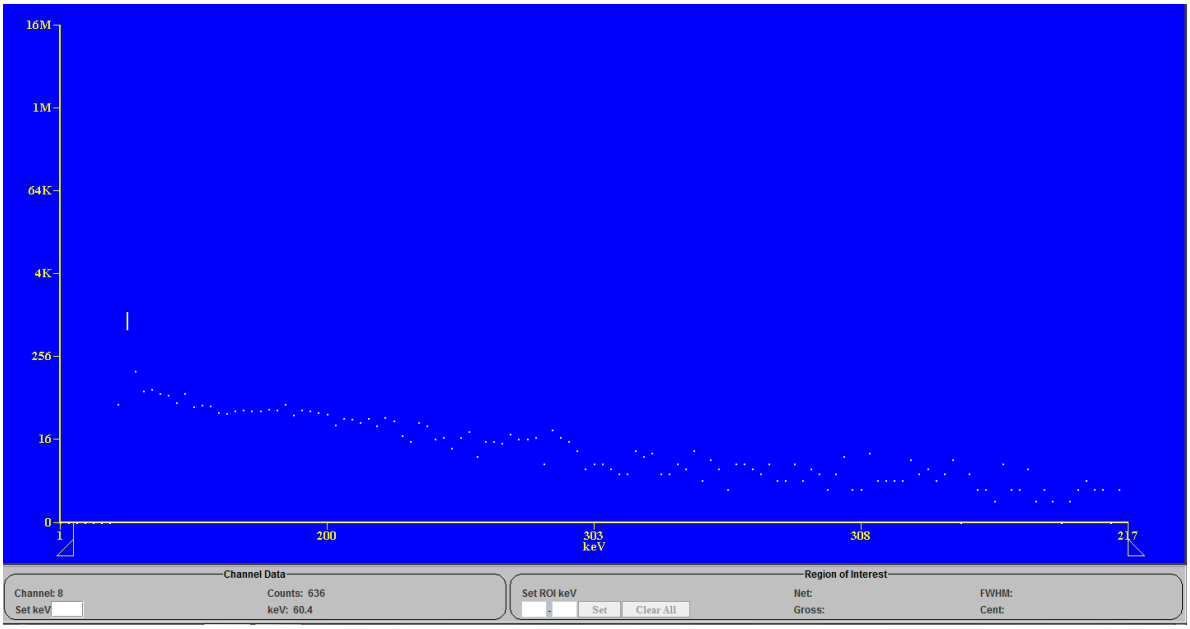

Figure 3.19: The photon spectrum for gamma rays, a) Am-241 only, b) passing through the memristor from Am-241

Chapter4
Conclusions and Future works

4.1 Conclusions

A low power micro-thick memristor with excellent retention and high R_{off}/R_{on} ratio of 10^7 has been proposed in this research. Both the low operating voltage range and the high endurance are unique electrical characteristics of this newly proposed memristor. It is the first micro-thick memristor with repeatable switching behavior based on the formation of a conductive bridge constructed from Ag ions. The micro-thickness of the memristor and the high R_{OFF}/R_{ON} encourage the investigation of the memristor's sensing capability. It has been found that the memristor, can be switched off during irradiation unlike the MOS transistor. Thus, this allows it to keep its excellent functionality without performance degradation. It has been also found that during Cs-137 irradiation, the memristor under small biased voltage switches on faster than in the absence of any irradiation event or even during the Am-241 irradiation. Actually, during the Am-241, the memristor is more active and switches faster than in the absence of any irradiation.

However, the gamma radiation interaction with the memristor might not be clearly measurable. To illustrate this, the photon radiation interactions depend on the thickness of the absorbing material. The dominant radiation interaction is referred to as the Compton scattering. This phenomenon occurs when a high energy photon hits a free electron resulting in both a scattered electron and a lower energy photon. Yet, the energy of the photon is still high enough resulting in a high transmission probability. Hence, it might be that the radiation passes through the matter without having the enough thickness to interact and transfer the energy to the material.

In this memristor, the TiO_2 is the metal oxide used. The element Ti has both a relatively low density and atomic number which signifies a lower radiation interaction. The high energy gamma radiation is more likely to propagate through the small metal oxide thickness which is around $45\mu m$ without affecting the material and the memristor's switching mechanism. Moreover, the randomness and the variations of the device are other factors that should be taken into consideration before concluding any possibility of radiation sensing. However, the DC bias test indicates that there are events that occur during the ionizing radiation

4.2 Future works

In order to optimize the memristor for radiation detection, the higher density, the atomic number as well as a material with higher thickness should be used. Hafnium is a material that can be used to design the memristor. Compared to Ti, it has high density and atomic number. Furthermore, another direction that ought to be taken into account in future studies is pushing the thickness of the active material to the maximum possible without losing the unique switching behavior. In addition, lower radiation photon energy radioactive materials can be used to study the radiation sensing capability such as Palladium-103, which has a mean gamma photon energy of 21keV. The active thickness with Hf oxide and the palladium is 0.022cm, which is less than what would be with Titanium oxide (0.3cm). Consequently, high atomic number materials with low photon energy radiation source are considered dominant factors for successful radiation detection.

References

[1] R. Bogue, "Developments in electromagnetic radiation sensing. Part one: short wavelengths," *Sensor Review*, vol. 31, no. 3, pp. 199 - 203, 2011.

[2] National Toxicology Program, "Ionizing Radiation," Department of Health and Human Services, USA, 2004.

[3] S. N. Ahmed, "Physics and Engineering of Radiation Detection," 1st ed. UK: Elsevier 2007.

[4] National cancer institute. (n.d). *Radiation Therapy for Cancer*.[online]. https://www.cancer.gov/about-cancer/treatment/types/radiation-therapy/radiation-fact-sheet

[5] E. B. Podgorsak, "Radiation Oncology Physics: A Handbook for Teachers and Students,"VIENNA: IAEA, 2005.

[6] American cancer society.(n.d). *X-rays, Gamma Rays, and Cancer Risk*.[online]. Avaliable: http://www.cancer.org/cancer/cancercauses/radiationexposureandcancer/xraysgammaraysandcancerrisk/x-rays-gamma-rays-and-cancer-risk-other-health-problems

[7] J. E. Turner, "Atoms, Radiation, and Radiation Protection," 3rd ed. New york: Wiley, 2007

[8] W. B. Mann, A. Rytz, A. Spernol, "Radioactivity measurements:Principles and Practice," Pergamon, 1991.

[9] A. Holmes-siedle and L. Adams, "Handbook of radiation effects," Oxford, 1993

[10] J. E. Turner, "Atoms, Radiation, and Radiation Protection," 3rd ed. New york: Wiley, 2007

[11] D. Broga, "Radiation Protection and Dosimetry: An Introduction to Health Physics" ,Springer,2008.

[12] S. N. Ahmed, "Physics and Engineering of Radiation Detection," 1st ed. UK: Elsevier 2007

[13] N. Tsoulfanidis, S. Landsberger, "Measurement and Radiation detection," 3rd ed. Taylar & Francis, 2011

[14] G. Knoll, "Radiation detection and measurement," 4th ed. New york: Wiley, 2010.

[15] C. Leroy, "Review of radiation detectors," in *AIP Conference Proceedings*, 01, pp. 49; 49-57; 57.

[16] M. Nikl, “Scintillation detectors for x-rays” in *Measurement Science and Technology,* 17(4), 2006.

[17] B. D. Milbrath, B. D. Milbrath, A. J. Peurrung, M. Bliss and W. J. Weber, "Radiation detector materials: An overview," *J. Mater. Res.*, vol. 23, pp. 2561; 2561-2581; 2581, /01/2008, 10.

[18] J. D. Reilly, N. Ensslh, H. smith, S. Kreiner, “Gamma-Rays Detector,” in *Passive Nondestructive Assay of Nuclear Materials,* City of Publisher, Country if not USA: Abbrev. of Publisher, 1991, ch. *3,* pp. *43–64.*

[19] J. R. Cooper, K. Randle and R. S Sokhi,” Radioactive releases in the environment : impact and assessment”, Chichester : John Wiley & Sons, 2003.

[20] Y. Ning, L. W Brady, "Radial Dose Function" in "Encyclopedia of Radiation Oncology", Springer Berlin Heidelberg: Berlin, Heidelberg, 2013.

[21] J. K. Author, “Detection of ionizating radiation ,” in *Journal of Physics E: Scientific Instruments*, 1976, pp.*233-251*.

[22] J. Seco, B. Clasie, M. Partridge, “Review on the characteristics of radiation detectors for dosimetry and imaging,” Institute of Physics and Engineering in Medicine, 2014, pp.*304-348.*

[23] J. Fraden, “Handbook of Modern Sensors : Physics, Designs, and Applications”, Springer, 2010.

[24] A. Ve´rtes, S. Nagy, Z. Klencsa´r, R. Lovas, F. Ro¨sch (Eds.), “Radiation Detection,” in *Handbook of nuclear chemistry, 2*nd ed. London: Springer, 2011, ch. *48*, pp. *2259–2286.*

[25] T. Gupta, “Radiation, ionization, and detection in nuclear medicine”, Heidelberg : Springer,2013G. Lutz, “Semiconductor Radiation detector,” 1st ed. New york: Springer, 2007

[26] A. Owens, "Semiconductor materials and radiation detection," *Journal of Synchrotron Radiation*, vol. 13, pp. 143; 143-150; 150, /01/2006, 03.

[27] D. K. Wehe,” Current Trends In Ionizing Radiation Detection”, *in Nuclear Engineering And Technology*, vol.38 no.4, 2006.

[28] E. B. Podyorask, “Radiation Oncology Physics:A Handbook For Teachers And Students,” Vienna, Austria : IAEA, 2005F. J. Ramírez-Jiménez and F. J. Ramírez-Jiménez, "PIN diode detectors," in *AIP Conference Proceedings*, 01, pp. 213; 213-226; 226.

[29] J. W. Jewett and R. A. Serway, *Scientists and engineers, chapters 1-22: Volume 1*, 8th ed. United States: Brooks/Cole, 2010.

[30] Mukherjee, B. and Makowski, D. and Krasinski, P. and Cross, P. and Grecki, M. and Simrock, S, "Novel applications of radiochromic film in radiation dosimetry at high-energy accelerators" in *2008 15th International Conference on Mixed Design of Integrated Circuits & Systems, 2008*

[31] G. Lutz, "Semiconductor Radiation detector," 1st ed. New york: Springer, 2007

[32] F. J. Ramírez-Jiménez and F. J. Ramírez-Jiménez, "PIN diode detectors," in *AIP Conference Proceedings,* 01, pp. 213; 213-226; 226

[33] R. P. P,1rker, "Semiconductor nuclear radiation detector," Physics in Medicine and Biology, Volume 15, Number 4, 1970

[34] M. F. L'Annunziata, "Handbook of radioactivity analysis," in *Handbook of Radioactivity Analysis*Anonymous Academic Press [Imprint], 2001.

[35] A.H. F. Muggleton, "Semiconductor devices for gamma ray, x-ray and nuclear radiation detection," Journal of Physics E: Scientific Instruments, Volume 5, Number 5, 1972

[36] Gábor Harsányi, "Sensors in Biomedical applications," *Sens Rev*, vol. 21, 12/01; 2016/08, 2001.

[37] G.Dearnaley, "Nuclear radiation detection by solid state devices*," Journal of Scientific Instruments*, Volume 43, Number 12, 1966.

[38] T. Kron, J. Lehmann and P. Greer, "Dosimetry of ionising radiation in modern radiation oncology", *Physics in Medicine and Biology*, vol. 61, no. 14, 2017.

[39] G. Aycik (Ed.), "Gas-Filled And Plastic Scintillation Detectors: Advantages And Disadvantages," in *New Techniques for the Detection of Nuclear and Radioactive Agents,* AA Dordrecht, The Netherlands: Springer, 2009, ch. *16*, pp. *181–192.*

[40] J. A. Victoreen, "Ionization Chamber," *Proceedings Of The I.R.E.* , pp. *189-199,* 1949

[41] L. Chua, "Memristor-The missing circuit element," *IEEE Transactions on Circuit Theory,* vol. 18, pp. 507-519, 1971.

[42] R. S. Williams, "How We Found The Missing Memristor," *IEEE Spectrum*, vol. 45, pp. 28-35, 2008.

[43] A. G.Radwan and, M. E. Fouda, "Memristor: Models, Types, and Applications", Springer International Publishing, 2015

[44] J. J. Yang, D. B. Strukov, and D. R. Stewart, "Memristive devices for computing," *Nature nanotechnology*, vol. 8, no. 1, pp. 13–24, 2013.

[45] L. Wang , C. Yang, J. Wen, S. Gai and Y. Peng, "Overview of emerging memristor families from resistive memristor to spintronic memristor," *J. Mater. Sci. : Mater. Electron.*, vol. 26, pp. 4618-4628, 07, 2015.

[46] P. Mohanty, "Memristor: From Basics to Deployment," *IEEE Potentials*, vol. 32, pp. 34-39, 2013.

[47] R. S. Williams, "How We Found The Missing Memristor," *IEEE Spectrum*, vol. 45, pp. 28-35, 2008.

[48] L. Chua, "Everything you wish to know about memristors but are afraid to ask," *Radioengineering*, vol. 24, pp. 319; 319-368; 368, 2015.

[49] D. S. Jeong, D. Jeong, R. Thomas, R. Katiyar and J. Scott, "Emerging memories: resistive switching mechanisms and current status," *Reports on Progress in Physics*, vol. 75, pp. 076502; 076502, /01/2012, 07.

[50] B. Mohammed, M. Abi Jaoude, V. Kumar, D. M. Al Homouz, H. Abu Nahla, M. Al-Qutayri, N. Christoforou," State of the art of metal oxide memristor devices Memristor," Nanotechnol Rev, 2015.

[51] J. J. Yang, M. D. Pickett, X. Li, D. A. A. Ohlberg, D. R. Stewart and R. S. Williams, "Memristive switching mechanism for metal/oxide/metal nanodevices," *Nature Nanotechnology*, vol. 3, pp. 429-433, 07, 2008.

[52] H. Abunahla, M. A. Jaoude, C. J. O'Kelly and B. Mohammad, "Sol-gel/drop-coated micro-thick TiO2 memristors for γ-ray sensing," *Mater. Chem. Phys.*, vol. 184, pp. 72-81, 12/1, 2016.

[53] E. Gale, R. Mayne, A. Adamatzky, and B. de Lacy Costello, "Drop coated titanium dioxide memristors," *Materials Chemistry and Physics*, vol. 143, no. 2, pp. 524–529, 2014

[54] R. Waser and M. Aono, "Nanoionics-based resistive switching memories," *Nature materials*, vol. 6, no. 11, pp. 833–840, 2007

[55] V. Rana and R. Waser, "Redox-based memristive devices," in *Memristors and Memristive Systems*. Springer, 2014, pp. 223–251.

[56] H. S. P. Wong *et al*., "Metal–Oxide RRAM," in *Proceedings of the IEEE*, vol. 100, no. 6, pp. 1951-1970, June 2012

[57] W. Lu, D. S. Jeong, M. Kozicki, and R. Waser, "Electrochemical metallization cells–blending nanoionics into nanoelectronics?" *MRS bulletin*, vol. 37, no. 2, p. 124, 2012.

[58] H. Barnaby, S. Malley, M. Land, S. Charnicki, A. Kathuria, B. Wilkens, E. DeIonno, and W. Tong, "Impact of alpha particles on the electrical characteristics of TiO_2 memristors," *IEEE Transactions on Nuclear Science*, vol. 58, no. 6, pp. 2838–2844, 2011.

[59] Y. Chi, R. Liu, Z. Tang, and R. Song, "Total ionizing dose effect on low on/off switching ratio TiO2 memristive memories," *IEEE Transactions on Nuclear Science*, vol. 61, no. 4, pp. 1889–1893, 2014

[60] M. L. McLain and M. J. Marinella, "Overview of the radiation response of anion-based memristive devices," in *Aerospace Conference, 2015 IEEE*. IEEE, 2015, pp. 1–11.

[61] D. R. Hughart, A. J. Lohn, P. R. Mickel, S. M. Dalton, P. E. Dodd, M. R. Shaneyfelt, A. I. Silva, E. Bielejec, G. Vizkelethy, M. T. Marshall *et al.*, "A comparison of the radiation response of TaOx and TiO2 memristors," *IEEE Transactions on Nuclear Science*, vol. 60, no. 6, pp. 4512–4519, 2013.

[62] M. J. Marinella, S. M. Dalton, P. R. Mickel, P. E. D. Dodd, M. R. Shaneyfelt, E. Bielejec, G. Vizkelethy, and P. G. Kotula, "Initial assessment of the effects of radiation on the electrical characteristics of TaOx memristive memories," *IEEE Transactions on Nuclear Science*, vol. 59, no. 6, pp. 2987–2994, 2012.

[63] D. R. Hughart, A. Lohn, P. R. Mickel, P. Dodd, M. Shaneyfelt, A. Silva, E. Bielejec, G. Vizkelethy, B. Doyle, M. T. Marshall *et al.*, "Radiation induced resistance changes in TaO_x and TiO_2 memristors," in *Aerospace Conference, 2014 IEEE*. IEEE, 2014, pp. 1–11.

[64] E. DeIonno and A. L. White, "Reliability considerations and radiation testing of memristor devices," in *Aerospace Conference, 2015 IEEE*. IEEE, 2015, pp. 1–6.

[65] W. M. Tong, J. J. Yang, P. J. Kuekes, D. R. Stewart, R. S. Williams, E. DeIonno, E. E. King, S. C. Witczak, M. D. Looper, and J. V. Osborn, "Radiation hardness of TiO2 memristive junctions," *IEEE Transactions on Nuclear Science*, vol. 57, no. 3, pp. 1640–1643, 2010.

[66] M. L. McLain, H. P. Hjalmarson, T. J. Sheridan, P. R. Mickel, D. Hanson, K. McDonald, D. R. Hughart, and M. J. Marinella, "The susceptibility of TaOx-based memristors to high dose rate ionizing radiation and total ionizing dose," *IEEE Transactions on Nuclear Science*, vol. 61, no. 6, pp. 2997–3004, 2014.

[67] NA, "Basic Physics of Nuclear Medicine/Attenuation of Gamma-Rays", last modified 2016

[68] T. Prodromakis, K. Michelakis and C. Toumazou, "Fabrication and electrical characteristics of memristors with TiO_2/TiO_{2+x} active layers," *Proceedings of 2010 IEEE International Symposium on Circuits and Systems*, Paris, 2010, pp. 1520-1522.

[69] D. M. Fryauf, K. J. Norris, J. Zhang, S. Y. Wang and N. P. Kobayashi, "Titanium oxide vertical resistive random-access memory device," in *IET Micro & Nano Letters*, vol. 10, no. 7, pp. 321-323, 7 2015. doi: 10.1049/mnl.2015.0021

[70] Navaneethan Duraisamy, Nauman Malik Muhammad, Hyung-Chan Kim, Jeong-Dai Jo, Kyung-Hyun Choi, "Fabrication of TiO2 thin film memristor device using electrohydrodynamic inkjet printing," Thin Solid Films, Volume 520, Issue 15, 31 May 2012, Pages 5070-5074

[71] M. hadi, "A New Resistive Switching Based on Breakdown and Anodic Re-Oxidation of Thin SiO2 at the Interface of CeOx Buffer Layer and Silicon Related Bottom Electrodes", Phd dissertation.

[72] Hu, SG and Wu, SY and Jia, WW and Yu, Q and Deng, LJ and Fu, Yong Qing and Liu, Y and Chen, Tu Pei, "Review of nanostructured resistive switching memristor and its applications", Nanoscience and Nanotechnology Letters: American Scientific Publishers, vol. 6, 2014

[73] I. Valov and M. N Kozicki, "Cation-based resistance change memory," Journal of Physics D: Applied Physics, 46 (7), 2013.

[74] L. Mahmoud, M. Abi Jaoude, M. Darweesh, H. Abunahla, G.e Hitt and B. Mohammad, "Low-Power and Highly Stable Microscale TiO2 Memristors for Gamma-Ray Sensing",The International Conference on Memristive Materials, Devices & Systems, MEMRISYS 2017)

[75] R. Waser, "Redox-based resistive switching memories," *Journal of nanoscience and nanotechnology*, vol. 12, no. 10, pp. 7628–7640, 2012.

[76] I. Valov, R. Waser, J. R. Jameson, and M. N. Kozicki, "Electrochemical metallization memories fundamentals, applications, prospects," *Nanotechnology*, vol. 22, no. 25, p. 254003, 2011.

[77] W. Lu, D. S. Jeong, M. Kozicki, and R. Waser, "Electrochemical metallization cells–blending nanoionics into nanoelectronics?" *MRS bulletin*, vol. 37, no. 2, p. 124, 2012.

[78] D. Ielmini, F. Nardi, and C. Cagli, "Universal reset characteristics of unipolar and bipolar metal-oxide rram," *IEEE Transactions on Electron Devices*, vol. 58, no. 10, pp. 3246–3253, 2011.

[79] Y. Chi, R. Liu, Z. Tang, and R. Song, "Total ionizing dose effect on low on/off switching ratio TiO2 memristive memories," *IEEE Transactions on Nuclear Science*, vol. 61, no. 4, pp. 1889–1893, 2014.

[80] M. L. McLain and M. J. Marinella, “Overview of the radiation response of anion-based memristive devices,” in *Aerospace Conference, 2015 IEEE*. IEEE, 2015, pp. 1–11.

[81] E. DeIonno and A. L. White, “Reliability considerations and radiation testing of memristor devices,” in *Aerospace Conference, 2015 IEEE*. IEEE, 2015, pp. 1–6.

[82] D. R. Hughart, A. J. Lohn, P. R. Mickel, S. M. Dalton, P. E. Dodd, M. R. Shaneyfelt, A. I. Silva, E. Bielejec, G. Vizkelethy, M. T. Marshall *et al.*, “A comparison of the radiation response of TaOx and TiO2 memristors,” *IEEE Transactions on Nuclear Science*, vol. 60, no. 6, pp. 4512–4519, 2013.

[83] M. J. Marinella, S. M. Dalton, P. R. Mickel, P. E. D. Dodd, M. R. Shaneyfelt, E. Bielejec, G. Vizkelethy, and P. G. Kotula, “Initial assessment of the effects of radiation on the electrical characteristics of TaOx memristive memories,” *IEEE Transactions on Nuclear Science*, vol. 59, no. 6, pp. 2987–2994, 2012.

[84] H. Barnaby, S. Malley, M. Land, S. Charnicki, A. Kathuria, B. Wilkens, E. DeIonno, and W. Tong, “Impact of alpha particles on the electrical characteristics of TiO_2 memristors,” *IEEE Transactions on Nuclear Science*, vol. 58, no. 6, pp. 2838–2844, 2011.

[85] W. M. Tong, J. J. Yang, P. J. Kuekes, D. R. Stewart, R. S. Williams, E. DeIonno, E. E. King, S. C. Witczak, M. D. Looper, and J. V. Osborn, “Radiation hardness of TiO2 memristive junctions,” *IEEE Transactions on Nuclear Science*, vol. 57, no. 3, pp. 1640–1643, 2010.

[86] M. L. McLain, H. P. Hjalmarson, T. J. Sheridan, P. R. Mickel, D. Hanson, K. McDonald, D. R. Hughart, and M. J. Marinella, “The susceptibility of TaOx-based memristors to high dose rate ionizing radiation and total ionizing dose,” *IEEE Transactions on Nuclear Science*, vol. 61, no. 6, pp. 2997–3004, 2014.

[87] Vandana A. Tupe[1] , P. P. Pawar[2], D.R. Shengule[3] and K M Jadhav[2], “Studies on Mass & linear attenuation coefficients of γ- rays of photons for Ag in the energy range 360-1330 keV,2012

[88] N.a , http://physics.nist.gov/PhysRefData/XrayMassCoef/tab3.html

Appendix A

This experiment should be repeated 280 days to have measurable effect, since the memristor thickness is small.

Geiger Miller counts

The aim of this experiment is to check if there is any effect of radiation on the memristor by observing the number of counts. The Geiger miller was used in this experiment to count the collected particles per minute. The counter is connected to software ST360 for timing setting and counts display. This experiment is divided into four stages. The first stage in this experiment is to study the background, thus, the detector was set to count the background effect or the surrounding effects (i.e empty without any radiation source or memristor) to have a count each 1 minute for 10 times. Then, the same experimental setups were done when the radiation source is placed inside the detector alone, and when the plastic substrates are placed inside detector on top of the radiation source. The last stage is when the memristor is placed on top of the radiation source, as shown in Figure 3.16. The average of these counters for the 4 experimental stages are listed in Table 3.7. The average counts for the background is small compared to other stages since the detector is empty. When the radiation source is placed in the detector, the counts number is increased which indicates that the particles are collected from the radiation source. The drop in the counts when the plastic substrates are placed on top of the radiation source indicates that the gamma ray is interacting with the plastic. However, this number does not change after placing the memristor instead of the plastic substrates. Thus, it can be concluded that the memristor is transparent to the gamma radiation while the radiation attenuates as it propagates through the plastic, due to its high thickness. From Figure 3.16, further confirmations that at each minute, the counts are the almost the same for the 10 minutes.

Table 1: GM counts for 4 stages using Cs-137 of photon energy 662keV.

Experimental Stages	**Stage 1: Background noise**	**Stage 2: Cs-137 only**	**Stage3: Cs-137 + plastic substrate**	**Stage4: Cs-137 + memristor**
Average counts	12.4±3.2	646.8 ±29.8	246.6± 21.9	247.6±15.8

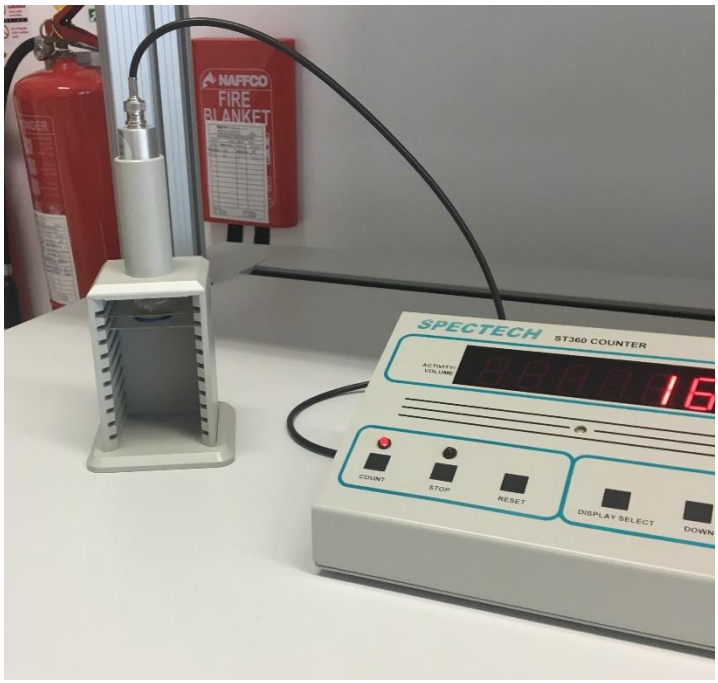

Figure 01: GM counter with memristor and the radiation source Cs-137

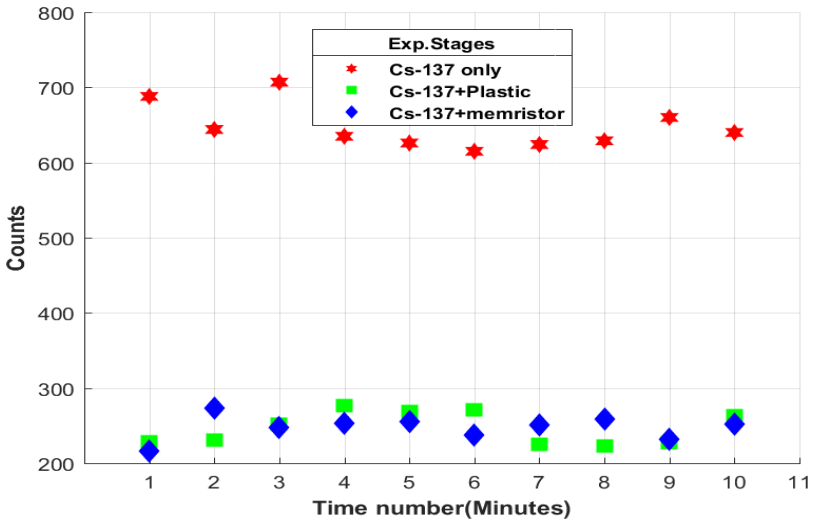

Figure 2: The number of counts at each minute for 10 minutes for the GM counting experiments